PSYCHOPHYSICAL AND ELECTROPHYSIOLOGICAL MEASURES OF LATERAL INTERACTIONS IN HUMANS

A thesis presented to the graduate faculty of
New England College of Optometry in partial fulfillment
of the requirements for the degree of Master of Science

Rachel K. Harmon
April 2025

PSYCHOPHYSICAL AND ELECTROPHYSIOLOGICAL MEASURES OF LATERAL INTERACTIONS IN HUMANS

Rachel K. Harmon

This manuscript has been read and accepted by the
Thesis Committee in satisfaction
of the thesis requirement for the degree of Master of Science

5/11/2025
Date

DocuSigned by:
Fuensanta Vera-Diaz
1502BB240B7D404...
Fuensanta A. Vera-Diaz, OD, PhD, FAAO
Graduate Faculty Advisor

DocuSigned by:
Peter Bex
3E92398B601647F...
Peter J. Bex, PhD
Thesis Committee Member

DocuSigned by:
Chris Taylor
8C96C99C286D4CA...
Christopher P. Taylor, PhD
Thesis Committee Member

DocuSigned by:
78A8AD972399447...
Athanasios Panorgias, MSc, PhD
Thesis Committee Member

5/11/2025
Date

DocuSigned by:
78A8AD972399447...
Athanasios Panorgias, MSc, PhD, FAAO
Director of Graduate Studies

Abstract

PSYCHOPHYSICAL AND ELECTROPHYSIOLOGICAL MEASURES OF LATERAL INTERACTIONS IN HUMANS

Rachel K. Harmon

New England College of Optometry

Introduction:

Lateral interactions are a key mechanism in visual processing and thought to be relevant in emmetropization. The present study addresses the relationship between axial length (AXL) and electrophysiological and psychophysical correlates of lateral interactions in the midperiphery.

Methods:

Subjects (n = 35; Age 25 ± 2 years; AXL 24.97 ± 1.17 mm) had no ocular pathology or vision deficits other than refractive error (spherical equivalent, M -2.97 ± 2.36 D). Contrast Sensitivity (CSF) and Threshold versus Contrast (TvC) curves were obtained at 6 deg or 10 deg eccentricity. TvC curves, investigating the effect of surround contrast on thresholds, were tested under both monocular and dichoptic conditions. Electroretinography (ERG) and Visual Evoked Potentials (VEP) were recorded in response to a novel stimulus generating a surround contrast versus response function for each subject. Spearman-Rank correlations were analyzed as a function of AXL (primary outcome) and M (secondary outcome).

Results:

Ocular biometry, refraction, and acuity: As expected, AXL and M exhibited a significant negative correlation ($R_s = -0.612$, $p < 0.001$).

CSF: No significant correlations were found between AXL and total area under the log CSF (AULCSF) at either eccentricity. A statistically significant negative correlation was found

between the area the low frequency dropoff (AULCSF_LowPass) and AXL at 10 deg (Rs = -0.463, p = 0.030). There was no relationship between AULCSF_LowPass and AXL at 6 deg. AULCSF (Rs = 0.475, p = 0.025) demonstrated significant positive correlations with M at 10 deg. No significant correlations were noted between AULCSF or AULCSF_LowPass and M at either 6 or 10 deg eccentricity. The high spatial frequency cutoff of the CSF (Acuity) was negatively correlated with AXL at 10 deg (Rs = -0.439, p = 0.044), but not 6 deg; coinciding with a positive correlation with M at 10 deg (Rs = 0.455, p = 0.034), but not 6 deg. Neither the spatial frequency at the CSF peak (SFpeak) nor the peak contrast sensitivity (CSpeak) were correlated with AXL or M at either eccentricity.

TVC: No significant correlations were noted for area under the TvC curve (AUTVC), Intrinsic Noise (IN), sensitivity to change in contrast (Psi), pedestal contrast at function minimum (MinPedes), or contrast threshold at function minimum (MinThresh) with either AXL or M at any eccentricity or testing condition.

Electrophysiology: No significant correlations were found between ERG/VEP results and AXL or M at either eccentricity for any surround contrast level.

Discussion:

This study supports a possible relationship between psychophysical measures of lateral interactions and axial length/refractive error. Lateral interactions contributing to the low spatial frequency dropoff of the CSF may be increased with increasing axial length, with a possible differential effect at 10 deg versus 6 deg. No significant relationships were found with either AXL or M in either psychophysical (TvC) or electrophysiological experiments investigating the effect of surround stimulation. Further work is needed to solidify our understanding of these interactions and where such relationships originate in the visual pathway.

Table of Contents

List of Figure and Table Legends

1. General Introduction

1.1 Introduction

As a leading cause of vision loss, myopia is a global public health concern [1,2]. In addition to causing defocus on the retina and blurry vision, myopia is associated with an increased risk of vision-threatening ocular pathologies such as retinal detachment, staphyloma, and myopic maculopathy [3]. Although myopia can be caused by an increase in the refractive power of the eye, it is most often caused by excessive ocular elongation [4–6]. Current research suggests that myopia, a failure of emmetropization, is the result of a combination of genetic and environmental factors [7–12]. Unfortunately, the underlying mechanism whereby the eye grows excessively long and therefore develops myopia is not well understood, especially at the cellular level. Much of the research to date focuses on identifying the external, environmental, factors involved in emmetropization, as well as intrinsic factors such as the optics of the eye and accommodation.

Axial elongation is caused by changes in the fibrous sclera, which is largely mediated by signals from the retina. A preponderance of evidence implicates the retina as the primary mediator of both defocus/growth signal detection and the origin of the subsequent signalling cascade [13–16]. However, there remains little research on the differential activity of retinal cell types in relation to myopia. A thorough understanding of the various cells in the visual pathway could further elucidate the pathophysiology of myopia development and promote novel therapeutic techniques. As part of a larger research project exploring the relationship between axial length and activity of retinal cells, this study seeks to investigate lateral interactions within the retina. Specifically, we focus on the activity of horizontal and amacrine cells as a function of axial length (AXL).

Horizontal cells (HC) are the basis for lateral inhibition, the mechanism that facilitates contrast enhancement and the formation of receptive fields [17–25]. With nuclei in the inner nuclear layer and synapses in the outer plexiform layer, HCs form lateral networks between photoreceptors and facilitate some of the earliest processing in the visual pathway [26,27]. In humans, their function is often studied through psychophysical analysis of contrast sensitivity at low spatial frequencies [18,28–33], which is known to be dictated by the lateral inhibitory function of the horizontal cells [34].

While there remains a gap in our understanding of the contribution of HCs to myopia development, recent work in animal models suggests that they may play an integral role in regulating normal eye growth and emmetropization [2,35,36]. For example, Barathi and colleagues pointed to disruption in GABA signaling as a potential mechanism for myopia control with atropine [35]. This suggests that horizontal cells and/or amacrine cells are involved in the regulation of eye growth since these cell types utilize GABA as a neurotransmitter. Li and colleagues found that calcium signaling by horizontal cells is significantly reduced in a mouse model of form-deprivation myopia [2]. Another group investigated the expression of long-coding RNAs in myopia and found colocalization of certain differentially expressed genes in retinal ganglion cells and horizontal cells [37]. Based on this work, horizontal cell signaling remains an interesting candidate for intraretinal processing in emmetropization.

Amacrine Cells (AC) are similarly involved in the integration of retinal signals laterally, connecting bipolar and ganglion cells in the inner plexiform layer [26]. Due to the high variability in AC function and morphology, the functions of these cells are not yet fully understood. However, they are thought to be associated with oscillatory potentials on electroretinogram waveforms that vary significantly between individuals and recording conditions [19]. Similar to

horizontal cells, current research in animal and genetic studies suggests that ACs may also contribute to emmetropization [38–46]. There is particular interest in the GABA-ergic and dopaminergic pathways within the retina, with several studies suggesting that amacrine cells may play a pivotal role [35,40–44,47]. Various structural studies point to thinning of the inner nuclear and outer plexiform later in myopia, which could be due to the loss of bipolar, amacrine, and/or horizontal cells with increasing axial length [48–50]. Careful analysis of AC as a function of AXL may help understand the potential role of amacrine cells in emmetropization.

Although lateral inhibition and receptive field development [17–20,23–25] have been thoroughly studied with regard to their physiological function in animal models, they are difficult to study in human subjects, resulting in a lack of research into their potential role in myopia development. Current research into lateral interactions revolves primarily around psychophysics studying lateral inhibition and contrast sensitivity [18,28–33] or animal models involving ex vivo analysis [2,35,36,51–54]. Additionally, psychophysical testing has been largely limited to the foveal region, prohibiting a complete understanding of retinal diseases with suspected peripheral involvement. While research into other retinal phenomena benefit from validated electroretinogram (ERG) protocols (23–29), there is no established method specifically designed to assess lateral interactions. To address these gaps in knowledge, ERG and Psychophysical paradigms were developed targeting lateral mechanisms through study of responses to custom center-surround stimuli.

We hypothesize that lateral interactions in the retina may be decreased by axial elongation without myopia-associated ocular pathology, possibly contributing to retinal dysregulation and myopia progression. Future studies may seek to determine whether differences seen in horizontal and amacrine cell function contribute to myopia development or are its result.

1.2 Specific Aims

This project aims to address the current deficit in our understanding of the role of lateral interactions in human myopia and how they correlate with axial length (AXL). A novel ERG paradigm and psychophysical methods were used for this purpose.

The specific aims of the study are:

AIM 1. To investigate the relationship between AXL and lateral interactions of HCs and ACs in the human retina.

The following measurements will be used:

- Photopic full-field flash ERGs for measurement of oscillatory potentials
- Custom-made stimulus for center-surround ERGs/VEPs
- Contrast Sensitivity Function (CSF) in the fovea and peripheral retina
- Center-Surround Contrast Thresholds in the fovea and peripheral retina under monocular and dichoptic conditions
- Ocular Biometry: AXL, anterior chamber depth, lens thickness, vitreous chamber depth, and keratometry
- Posterior segment High-Resolution Wide-Field Ocular Coherence Tomography (OCT) of the retina and choroid

It is hypothesized that increased AXL will be systematically associated with decreased lateral interactions measured via ERGs and psychophysical methods.

AIM 2: To investigate the relationship between retinal eccentricity and lateral interactions of HCs and in the human retina.

The following measurements will be used:

- Photopic and scotopic Full-Field flash ERGs for the measurement of oscillatory potentials
- Multifocal ERGs for a range of background luminances in photopic conditions
- CSF in the fovea and peripheral retina
- Center-Surround Contrast Thresholds in the fovea and peripheral retina under monocular and dichoptic conditions
- Ocular Biometry: AXL, anterior chamber depth, lens thickness, vitreous chamber depth, and keratometry
- Posterior segment High-Resolution Wide-Field OCT of the retina and choroid

It is hypothesized that retinal eccentricity will be systematically associated with the magnitude of lateral interactions as measured via ERG waveforms and psychophysical methods.

For both Aims, results from psychophysical testing will be qualitatively compared with the results from electroretinography to facilitate a clearer understanding of the relationship between lateral interactions and AXL. Understanding these interactions may inform our understanding of myopia progression and management techniques.

1.3. Subjects

Inclusion criteria for participation in this study were: (1) within 18 and 32 years of age, (2) best-corrected logMAR VA (BCVA) ≤ +0.10 (20/20 equivalent) or better in each eye, (3) spherical equivalent refractive error (M) between +5.00 and -7.00 Diopters in each eye with a cylinder value no larger than 2.50 Diopters, (4) no history of ocular surgery or disease that may

have resulted in visual consequences, (5) not using ocular or systemic drugs that may affect their vision, (6) no strabismus or near vision binocular abnormalities, (7) not pregnant or nursing, (8) no history of allergy to any eye drops, (9) no history of seizures or diagnosis of epilepsy, and (10) able to provide verbal or written informed consent. Subjects were recruited within the NECO population via email outreach. This study was approved by the Institutional Review Board (IRB) of New England College of Optometry (NECO), Boston, Massachusetts. The research was conducted in accordance with the tenets of the Declaration of Helsinki. Informed consent was obtained from each subject after an explanation of procedures and risks and prior to any testing.

1.4. Schedule of Collaborative Data Collection

A cross-sectional study was conducted during four visits, including measures of retinal structure, cellular function, and visual performance. This was a collaborative data collection process with three other MS students (Raviv Katz, Srini Srirangam, and Simon Wong). Within the following schedule, measures utilized in the present analysis are underlined.

- Visit 1: Informed Consent, Vision Screening, Psychophysics probing the Contrast Sensitivity (CS) of Bipolar Cells, Optical Coherence Tomography (OCT), and Ocular Biometry (Lenstar).
- Visit 2: Psychophysics probing the Contrast Sensitivity Function (CSF) in the Fovea and Periphery, Psychophysics probing Center-Surround Contrast Thresholds in the Fovea and Periphery, Rod-isolating Electroretinography (ERG), Paired-Flash Cone ERG, Paired-Flash Rod ERG.

- Visit 3: Psychophysics probing CS with chromatic and temporal modulation, Ganglion Cell ERG, Background Contrast vs Response Pattern ERG, Bipolar Cell ERG, Visual Evoked Potentials.
- Visit 4: Psychophysics probing the recovery rate of photoreceptors, Psychophysics probing the CS Bipolar Cells, Ocular Biometry (Lenstar).

1.5. Vision Tests

At the initial visit, subjects underwent a thorough vision screening to determine inclusion eligibility. The following measures were taken to screen for ocular health: (1) comprehensive health and ocular history, (2) lensometry of habitual distance optical correction, (3) distance and near clinical visual acuity using a computerized logMAR chart, (4) estimated distance and near cover test, (5) near point of convergence with an accommodative target, (6) counting fingers confrontation visual fields, (7) measurement of pupil reactivity and sizes using a transilluminator and ruler, (8) extraocular muscles assessment, (9) rebound tonometry using an iCare ic100 tonometer, (10) dynamic retinoscopy using the monocular estimated method, (11) static distance retinoscopy, and (13) slit lamp anterior segment health evaluation. In conjunction with the vision screening, the following measures were acquired as part of the study's data set (13) biometry using Lenstar, (14) optical coherence tomography (OCT), and (15) objective refraction with static retinoscopy and a WAM open-field autorefractor, to determine the subjects' refractive error. If visual acuity through objective refraction was not sufficient to achieve logMAR VA of +0.10 or better, (16) distance subjective refraction with binocular balance was performed to determine refractive error. Power vectors M, J_0, and J_{45} were calculated from the refractive error determined using either WAM if the subject reached +0.10 logMAR acuity through this correction or subjective refraction if they did not reach +0.10 logMAR with the WAM findings.

The spherical equivalent refractive error (M), calculated as the spherical power plus one-half the cylinder power in diopters (S - C/2), was used for subsequent statistical analyses [55]. J_0 was calculated as (-C/2)[cos(2(β - 90)] and J_{45} as (-C/2)[sin2(β - 90)], as described by Thibos et al. [55]. Future psychophysical and electroretinography tasks were performed through appropriate refractive correction determined during this initial testing, as indicated.

Ocular biometry measurements were taken using the Lenstar LS900 [https://www.haag-streit.com/]. Five measurements were taken from each eye to obtain AXL, anterior chamber depth (ACD), and lens thickness (LT). These data were used to (1) determine the correlation of AXL and M between subjects, and (2) evaluate changes in AXL within subjects. A Heidelberg Spectralis OCT was used to obtain posterior segment high-resolution wide-field OCT in the right eye using two custom x6 radial scans using the 30-deg lens. These were recorded: (1) with enhanced depth imaging (EDI, ART 20 or 30, the higher the better resolution), and (2) without EDI (16A RT).

1.6. Statistical Analysis

This exploratory study sought to identify possible relationships between lateral mechanisms in the human retina and AXL. A multifaceted analysis was used to correlate measures of lateral processing (mediated in large part by HCs and ACs) with AXL as primary endpoints. Secondary analyses correlated the same measures with M. All analyses were conducted using Spearman's Rho due to many data sets containing non-parametric distributions. For each outcome, p-values are adjusted using a Bonferroni method to account for the same measurements being taken at two eccentricities: 6 and 10 deg from fixation. Data points greater

than 150% of the interquartile range outside of the upper and lower quartiles were considered outliers and were excluded from the analysis.

The experiments performed in this study fall into three categories: (1) psychophysical testing which produced the Contrast Sensitivity Function (CSF), (2) psychophysical testing which produced the Threshold versus Contrast function, and (3) electrophysiological responses to our custom stimulus. For each of these categories, an unconventional alpha cutoff was determined as a threshold for identifying "interesting" results that may warrant follow-up studies. This unconventional alpha cutoff, that is one greater than $\alpha < 0.05$, was determined by solving the equations for power for alpha rather than a sample size for a fixed power (a traditional a priori power analysis). To be specific:

(1) Power (1- β) was set to 80%

(2) N was the sample size we were able to obtain during the MS project, which was the number of subjects deemed complete cases (i.e., the subject had data in all conditions, after drop-out and outlier removal via Tukey's criterion [56,57]

(3) Selected the maximum effect size we observed among our Spearman Rank correlations.

From the calculations, we determined that an unconventional alpha of 0.1 would be used for outcomes extracted from the CSF. For outcomes extracted from the TvC function, an unconventional alpha of 0.2 was used. For outcomes extracted from ERG/VEP responses, an unconventional alpha of 0.40 will be utilized. The purpose of this unconventional secondary analysis is to provide guidance for future research projects that investigate lateral interactions within the visual system. Also note, by increasing the alpha cut-off the reader should keep in mind we are effectively saying, "we are willing to tolerate a false-alarm or type I error at a level greater than the 1/20 ($\alpha <= 0.05$) that is conventionally used in our sub-field."

Differences between group means were analyzed for comparisons made between eccentric locations. For CSF results, a one-way ANOVA was used to compare eccentric locations. For TVC results, Two-way ANOVA was used to assess differences between eccentric locations, monocular vs dichoptic testing methods, and interaction effects. For ERG and VEP results, Two-way ANOVA was utilized to assess differences between eccentric locations, pedestal contrast levels of the surround, and interaction effects. Tukey's post hoc analysis was performed if statistical significance was found in the initial ANOVA. With respect to ANOVA, a traditional cutoff of 0.05 was used to identify significant differences between specified testing conditions and/or eccentricities. Analysis was conducted using the R programming language in RStudio (https://posit.co/download/rstudio-desktop/).

1.7. General Results

Young adult subjects aged 22 - 32 years (25.00 ± 2.22) (n = 35) underwent a thorough vision screening (Table 3.1). All subjects had distance BCVA +0.10 logMAR (20/25 Snellent equivalent) or better in each eye and no ocular pathology or vision deficit other than refractive error, per the inclusion criteria. AXL was obtained in the right eye only using the Lenstar optical biometer as the average of 5 measures. AXL was the primary correlation of interest in this project (24.974 ± 1.167 mm, range 22.500 to 27.510 mm) (Table 4.1). Spherical equivalent refractive error (M -2.972 ± 2.362 D, range -6.875 to +1.150 D) was measured through non-cycloplegic open-field autorefraction values if distance VA was at least 20/25 with this correction; otherwise, a subjective refraction was also performed by a skilled examiner to achieve a DVA of 20/25 or better after refraction (Table 4.1). For analysis purposes, the calculated M value was used from either the objective autorefraction or the subjective refraction, as indicated. Correlations with M were considered secondary outcomes.

AXL and M values were normally distributed as determined using the Shapiro-Wilk normality test ($p = 0.915$ and $p = 0.070$, respectively). The majority of the other data sets in the study exhibited a non-normal distribution. For consistency, a Spearman-Rank Correlation was used throughout the analysis reported here. Using a traditional alpha cutoff of 0.05, AXL was significantly correlated with M using Spearman Rank Correlation analysis ($Rs = -0.612$, $p < 0.001$) (Figure 4.1), consistent with anticipated results.

Table 1.1. Summary of vision testing including Mean, Standard Deviation (SD), Minimum (Min), and Maximum (Max) of selected measures. All parameters are reported with 3 digits of precision.

Variable	Unit	Mean	SD	Min	Max
Age	yrs	25.000	2.223	22.000	32.000
Pupil_Size_Dim	mm	5.514	1.032	2.000	7.000
Pupil_Size_Bright	mm	3.264	0.770	1.500	5.000
IOP	mmHg	15.111	2.388	10.000	20.000
MEM	D	0.516	0.242	0.000	1.000
M	D	-2.972	2.362	-6.875	1.150
J0	D	0.279	0.328	-0.400	1.000
J45	D	0.012	0.188	-0.500	0.440
Aniso	D	0.394	0.357	0.000	1.380
AXL	mm	24.974	1.167	22.500	27.510
CCT	um	542.111	26.845	487.000	597.000
ACD	mm	3.543	0.354	2.830	4.180
LT	mm	3.612	0.173	3.180	4.040
K1	D	42.949	1.597	39.470	45.820
K2	D	43.989	1.620	40.780	47.110

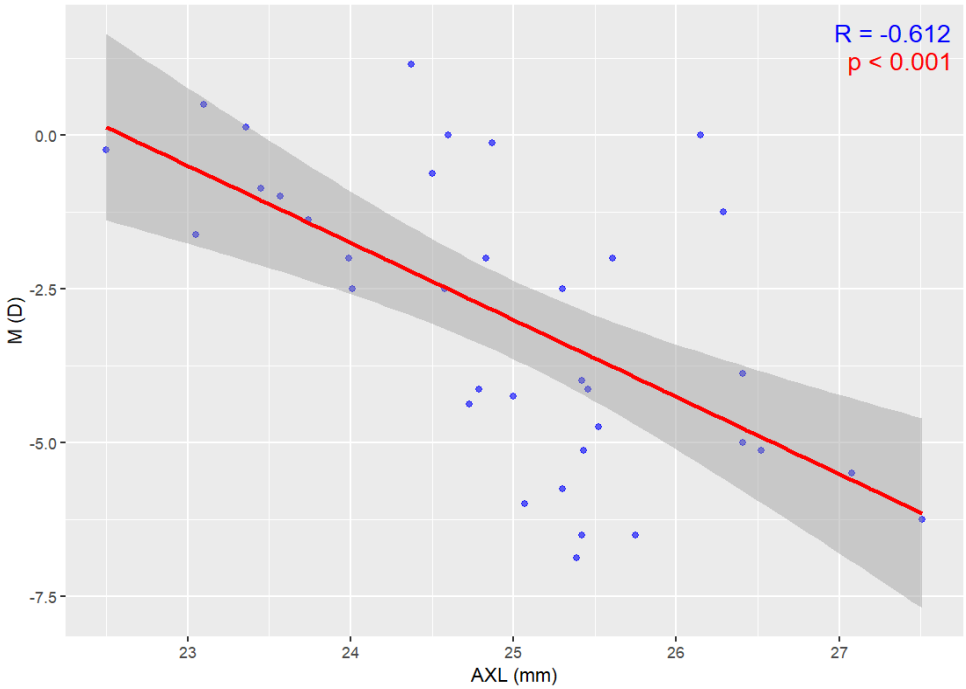

Figure 1.1. Scatter plot assessing the relationship between axial length (AXL) and spherical equivalent refractive error (M). A significant negative correlation was found between AXL and M (Rs = -0.612, $p < 0.001$).

2. Experiment 1: Contrast Sensitivity Function (CSF)

2.1 CSF Methods

Full CSFs were measured for each subject for their right eye. Spearman Rank correlations were analyzed to determine the relationship between each specific measure with AXL and M.

Custom MATLAB software programmed by Dr. Peter J. Bex (NorthEastern University) was used to measure the CSF at three retinal regions: 0-4, 4-8, and 8-12 deg eccentricity from the fovea. Targets were sine-wave luminance gratings with randomly varying contrast (range = 0.001 - 1) and spatial frequency (range = 0.25 - 40 cpd). Targets were circular, spanning 4 deg visual angle diameter and having a Gaussian profile (fading toward the edges).

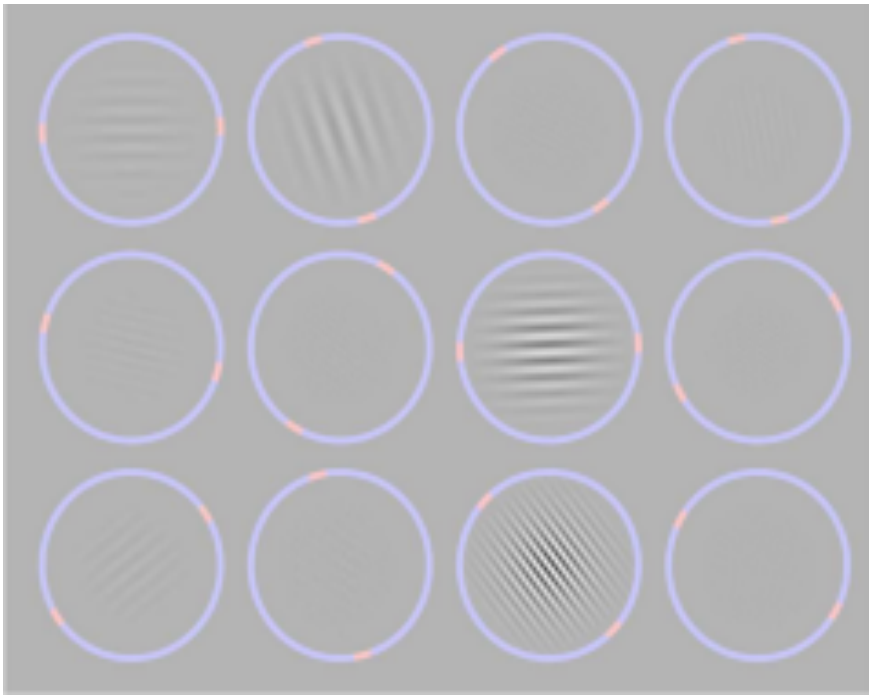

Figure 2.1. Representative stimulus for the foveal (0 deg) CSF experiments. Upon selecting orientation of stimulus, pink areas appear to indicate position chosen by subject. In this example, the subject has already selected the orientation of all stimuli.

For foveal targets (0 deg), stimuli were presented 12 at a time in a 3 x 4 array over 4 screens, totaling 48 stimuli (Figure 2.1). Subjects were able to look freely at each stimulus in turn (thereby utilizing their fovea for vision) and were asked to select the orientation of the grating using a mouse as they glanced from target to target. Subjects wore appropriate spectacle correction as indicated above. The angular error was determined by the difference between the selected and actual orientations of the stimulus.

For the peripheral CSF experiment, only one stimulus was presented at a time for 100 ms at one of 8 spatial locations while the subject fixated on a central point (Figure 2.2). The ring of possible locations was located at either 6 or 10 deg eccentricity depending on the trial. Gaze tracking (Gazepoint GP3) was utilized to ensure that the stimulus only appeared when the subject was looking at the central fixation point. Subjects were asked to select the peripheral location where the stimulus was presented.

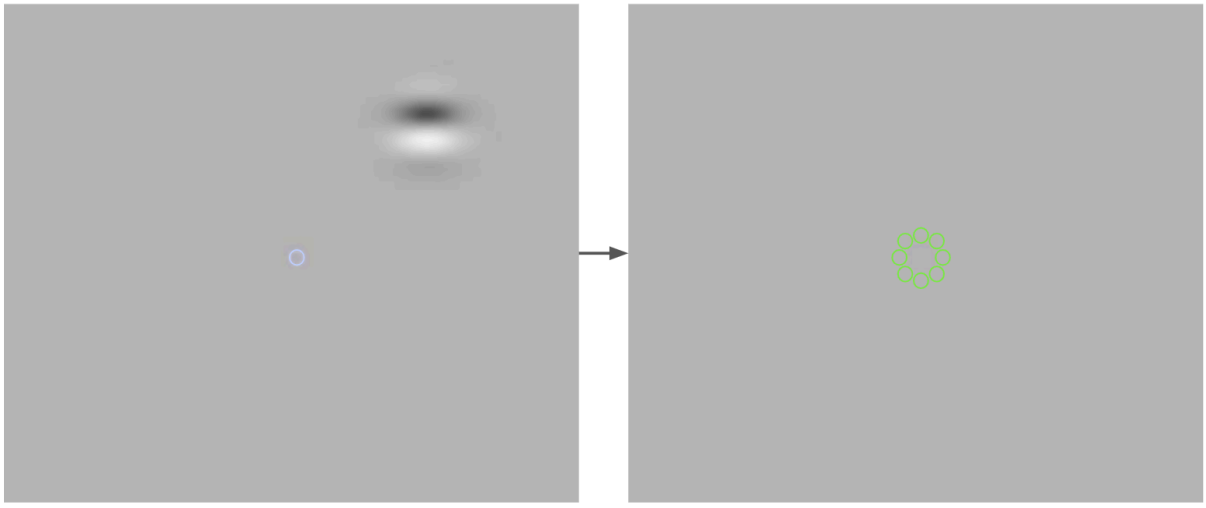

Figure 2.2. Representative stimulus for the peripheral CSF experiment tested at 6 deg. On the left, the light, central circle represents the fixation target, while a high contrast target is presented in one of 8 possible locations surrounding fixation. The right image represents the response ring that appears after stimulus presentation. Once the subject selects one from the 8 green circles in the response ring, the next stimulus is presented, and the cycle repeats.

Both experiments utilized a modified staircase method to determine the spatial frequency and contrast of subsequent stimuli, with a maximum of 48 trials at each eccentricity. Experiments were conducted under photopic conditions.

2.2 CSF Results

The Contrast Sensitivity Function (CSF) was measured monocularly in the right eye only, with the left eye fogged using a frosted lens. At each peripheral eccentricity, CSF curves were generated in MATLAB to achieve the best estimate of the true curve based on the data obtained (Figures 2.3 and 2.4). From these curves, the following data points were extracted: (1) total area under the logCSF curve (AULCSF), (2) area under the low frequency dropoff of the logCSF curve (AULCSF_LowPass), (3) acuity, (4) peak spatial frequency, and (5) peak contrast sensitivity. Spearman Rank correlations were performed relating these outcomes with AXL (primary outcome) and spherical equivalent (M) refractive error (secondary outcome).

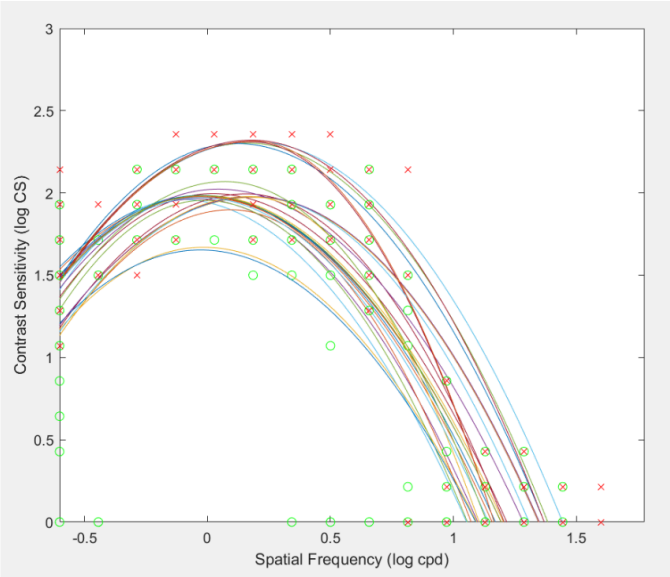

Figure 2.3. Contrast Sensitivity Function (CSF) curve fits for all subjects measured at 6 deg eccentricity in the peripheral retina. Both axes are plotted in logarithmic notation. Green circles represent data points where the subjects correctly identified the stimulus location, whereas red X data points represent trials where subjects incorrectly identified the location.

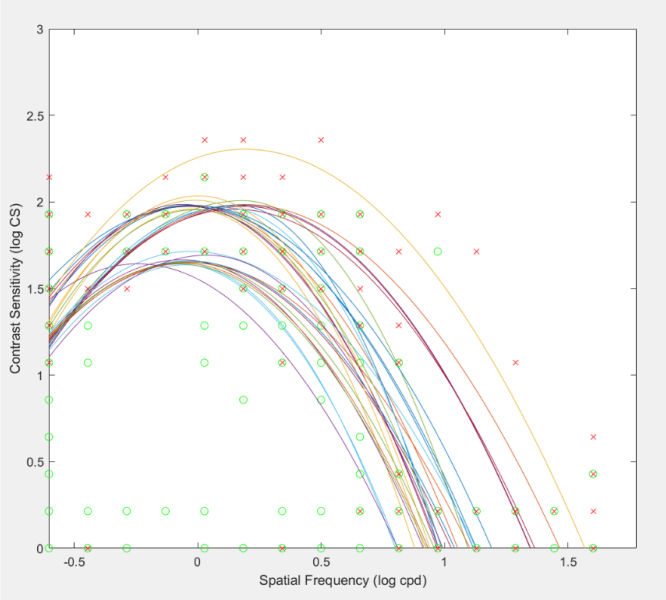

Figure 2.4. Contrast Sensitivity Function (CSF) curve fits for all subjects measured at 10 deg eccentricity in the peripheral retina. Both axes are plotted in logarithmic notation. Both axes are plotted in logarithmic notation. Green circles represent data points where the subjects correctly identified the stimulus location, whereas red X data points represent trials where subjects incorrectly identified the location.

After selecting complete data sets and removing outliers, 27 subjects were included in the analysis of the CSF. For each outcome, p-values are adjusted using the Bonferroni method to account for measurement at two eccentricities (6 and 10 deg). One-way ANOVA was performed to assess differences between 6 and 10 deg (Figure 2.5). Significant differences were found between eccentric locations for AULCSF (Mean 6 deg 3.141 +/- 0.399, 10 deg 2.651 +/- 0.460, $p < 0.001$), AULCSF_LowPass (Mean 6 deg 1.992 +/- 0.134, 10 deg 1.810 +/- 0.193, $p < 0.001$), Acuity (Mean 6 deg 16.802 +/- 4.654, 10 deg 12.772 +/- 7.446, $p = 0.021$), and CSpeak (Mean 6 deg 2.030 +/- 0.176, 10 deg 1.849 +/- 0.186, $p < 0.001$). For each of these outcomes, the group mean was higher at 6 deg than at 10 deg eccentricity (Table 2.1). No statistically significant difference was found for SFpeak between eccentric locations (Mean 6 deg 1.212 +/- 0.278, 10 deg 1.075 +/- 0.286). Overall, subjects were more sensitive to contrast (AULCSF and

AULCSF_LowPass) at 6 deg than at 10 deg, which is expected based on known characteristics of retinal structure. It was also expected that subjects would have greater maximum spatial frequency resolution at 6 deg than at 10 deg (Acuity), which is consistent with the present results. A difference in the location of the CSF peak (SFpeak and CSpeak) was also expected, but was not observed in this sample. This may be because (1) the two tested eccentricities are very close together or (2) the resolution of the ANOVA was not enough to detect a difference between the two eccentricities.

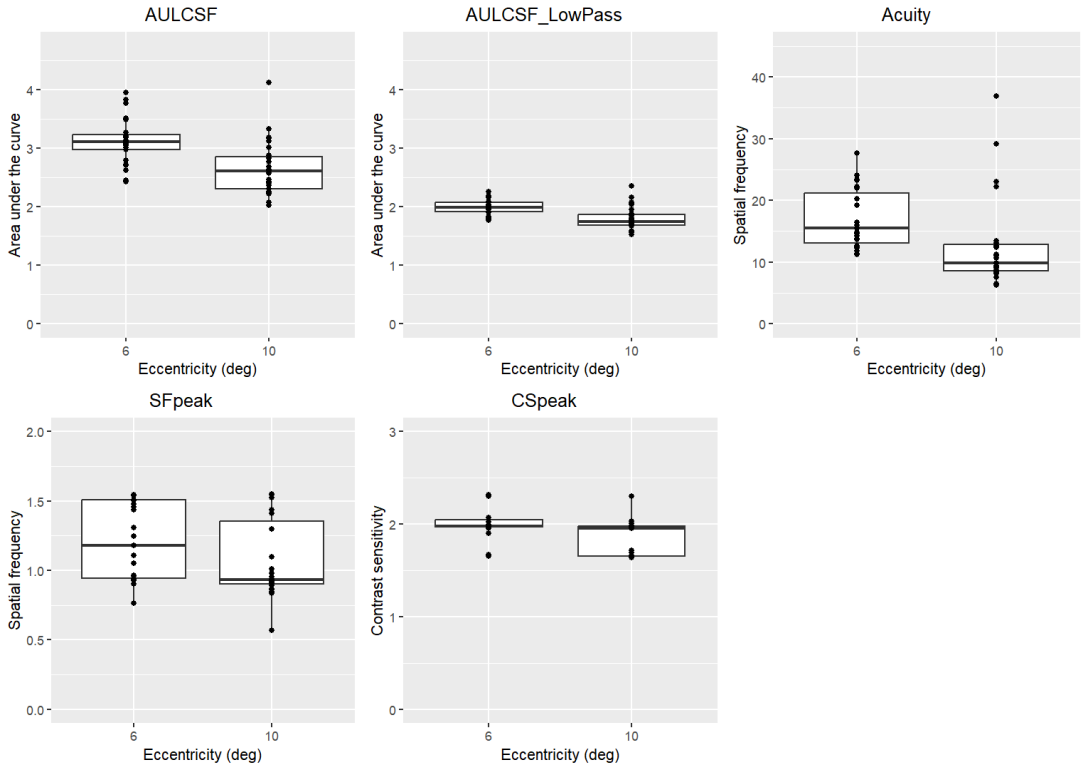

Figure 2.5. Comparison of CSF outcomes at 6 and 10 deg using one-way ANOVA. Significant differences were found between eccentric locations for AULCSF ($F = 17.5$, $p < 0.001$), AULCSF_LowPass ($F = 16.1$, $p < 0.001$), Acuity ($F = 5.69$, $p = 0.021$), and CSpeak ($F = 13.5$, $p < 0.001$). For all significant differences, the results were higher at 6 deg than at 10 deg eccentricity. No statistically significant difference was found for SFpeak between eccentric locations ($F = 3.18$, $p = 0.081$). Significance levels are as follows: *** $p < 0.001$, ** $p < 0.01$, * $p < 0.05$. All parameters are reported with 3 digits of precision.

Table 2.1. Summary Statistics for CSF outcomes separated by eccentricity. All parameters are reported with 3 digits of precision.

Variable	Eccentricity	Mean	SD	Min	Max
AULCSF	6	3.141	0.399	2.428	3.959
AULCSF	10	2.651	0.460	2.027	4.127
AULCSF_LowPass	6	1.992	0.134	1.769	2.265
AULCSF_LowPass	10	1.810	0.193	1.527	2.363
Acuity	6	16.802	4.654	11.272	27.641
Acuity	10	12.772	7.446	6.290	36.844
SFpeak	6	1.212	0.278	0.764	1.546
SFpeak	10	1.075	0.286	0.569	1.549
CSpeak	6	2.030	0.176	1.653	2.321
CSpeak	10	1.849	0.186	1.637	2.305

a. Area Under the Curve

The area under the curve was calculated twice for each subject: (1) including the entire area (AULCSF), and (2) assessing the area under the low-frequency dropoff (AULCSF_LowPass). AULCSF_LowPass was isolated using a low-pass filter set at 0.5 cpd. The cutoff of 0.5 cpd was utilized so as to exclude the peaks of all CSF functions at both 6 and 10 deg eccentricity. The lowest peak spatial frequency (SFpeak) was recorded at 10 deg eccentricity with a value of 0.569 cpd (Table 2.1). It was determined that a single spatial frequency cutoff would be more appropriate for standardization purposes than the peak of each individual's curve. Both AULCSF and AULCSF_LowPass were plotted against AXL (Figure 2.6) and M (Figure 2.7).

One-way ANOVA revealed significant differences between AULCSF at 6 and 10 deg eccentricity ($F = 17.5$, $p < 0.001$), with area under the curve being higher at 6 than at 10 deg. A similar relationship was noted for AULCSF_LowPass, where the area under the curve was greater at 6 than at 10 deg ($F = 16.1$, $p < 0.001$) (Figure 2.5, Table 2.1).

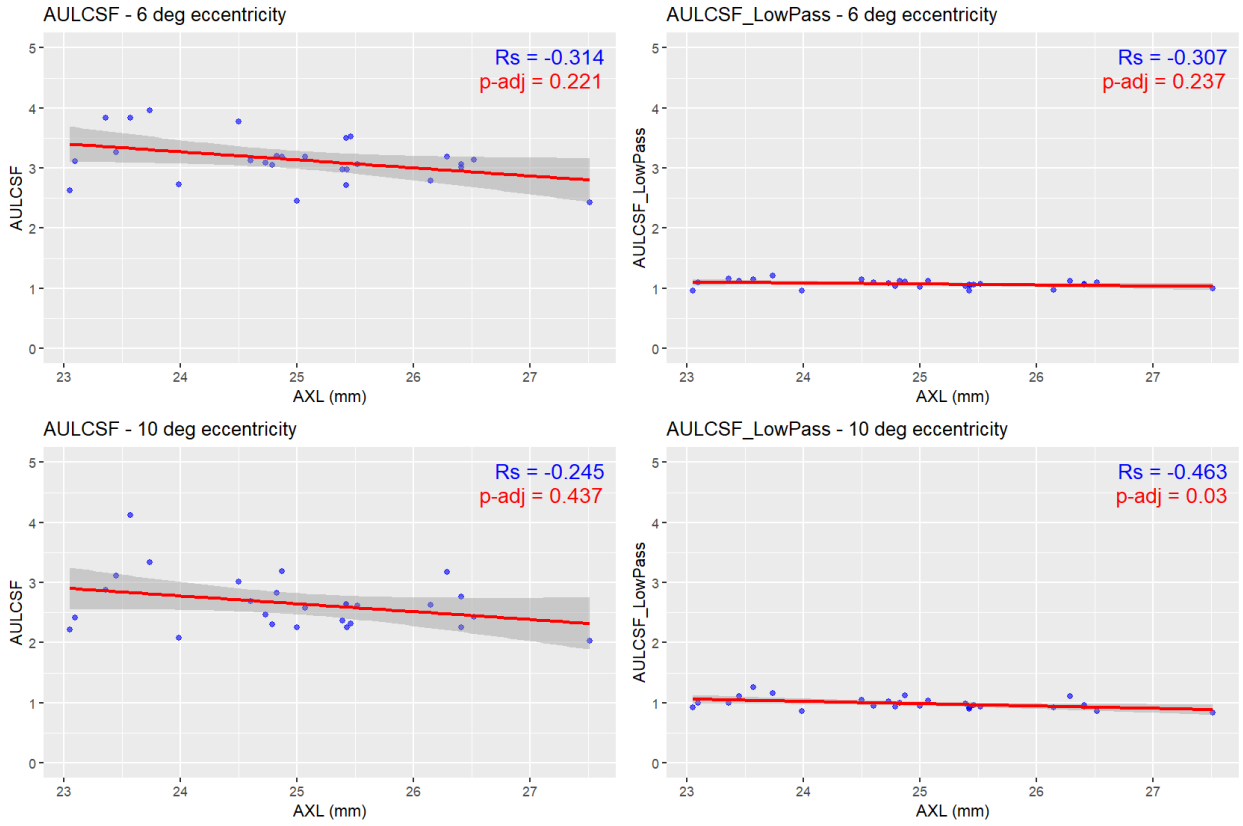

Figure 2.6. Spearman rank correlation of area under the CSF and axial length (AXL). Area under the entire logCSF (AULCSF) and area under the low frequency dropoff (AULCSF_LowPass; < 0.5 cpd) plotted as a function of axial length at 6 and 10 deg eccentricity. A promising relationship was noted between AXL and AULCSF_LowPass at 10 deg eccentricity (Rs = -0.463, p = 0.030), but not at 6 deg (Rs = -0.307, p = 0.237). No other correlations met the unconventional $\alpha < 0.10$. P-values are adjusted for two eccentricities using Bonferroni method and reported to three digits of precision.

No statistically significant correlations were found between the total AULCSF and AXL at either 6 or 10 deg eccentricity using a traditional alpha cutoff of 0.05. However, a significant negative correlation was found between AULCSF_LowPass and AXL at 10 deg eccentricity (Rs

= -0.463, p = 0.030), but not at 6 deg (Rs = -0.307, p = 0.237) (Figure 2.6). Recall that in section 1.6 we defined a calculation for setting α for "interestingness" which we called an unconventional alpha cut-off to have an algorithm for determining which results in this thesis seem promising for future investigation. Using our unconventional alpha of 0.1, only the correlation between AULCSF_LowPass and AXL at 10 deg eccentricity meets this criterion (Rs = -0.388, p = 0.091), where the area under the low frequency dropoff is lower in longer eyes.

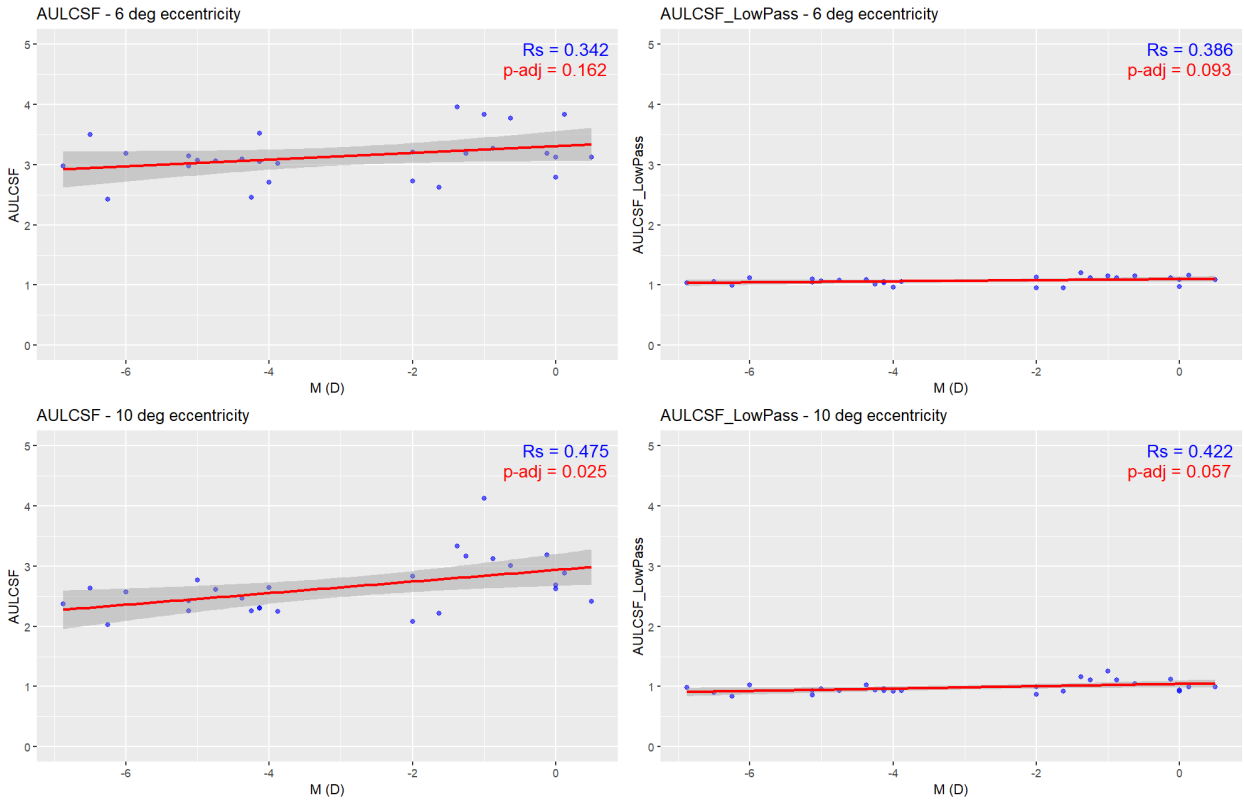

Figure 2.7. Spearman rank correlation of area under the CSF and spherical equivalent refractive error (M). Area under the entire logCSF (AULCSF) and area under the low frequency dropoff (AULCSF_LowPass; < 0.5cpd) plotted as a function of spherical equivalent refractive error (M) at 6 and 10 deg eccentricity. Significant positive correlations were noted at 10 deg eccentricity for AULCSF (Rs = 0.475, p = 0.025), but not AULCSF_LowPass . Correlations of AXL with AULCSF_LowPass met the unconventional alpha cutoff for promising results at both 6 deg (Rs = 0.386, p = 0.093) and 10 deg (Rs = 0.422, p = 0.057) eccentricity. P-values are adjusted for two eccentricities using Bonferroni method and reported to three digits of precision.

This is notable given that the correlation with total AULCSF at 10 deg is not sufficiently strong to reach the same level of interest. This is surprising and interesting, because the two measures are inherently linked. A true separation between AULCSF and AULCSF_LowPass would indicate that there is a differential effect happening at low spatial frequencies that is distinct from the overall pattern of the CSF curve. Such a distinction would be in line with previous work that emphasizes the importance of lower spatial frequencies in emmetropization [58–60]. However, it may also be that the current study simply lacks sufficient resolution to identify a relationship between AULCSF and AXL at 10 deg. In follow up studies, alternative methods for assessing the low spatial frequency cutoff should be explored that are less inherently linked with AULCSF. Current analysis uses a symmetric approximation for the contrast sensitivity function, which prevents the "splaying" of one side of the function independent of the other.. However, the effect we are hoping to measure whereby the low frequency region may be differentially affected by axial length may be better analyzed using an asymmetric CSF analysis. Using an asymmetric curve, it may be useful to extract a curve fit parameter which measures the rate of dropoff of the function which, taken together with analysis of the area under the curve, may provide an improved assessment of the relationship between axial length and the contrast sensitivity at the low-frequency dropoff.

Analysis of M as the secondary outcome also showed a positive correlation with AULCSF at 10 deg (Rs = 0.475, p = 0.025), where more myopic eyes tended toward lower overall contrast sensitivity. No relationship between AULCSF and M was noted at 6 deg eccentricity (Rs = 0.342, p = 0.162). Using the unconventional $\alpha < 0.1$, we also find that AULCSF_LowPass was correlated with M at both 10 deg (Rs = 0.422, p = 0.057) and 6 deg eccentricity (Rs = 0.386, p = 0.093); though the correlation appears stronger at 10 deg (Figure

2.7). This is especially interesting because of work that suggests that the near-periphery may play an important role in the emmetropization process [61] .

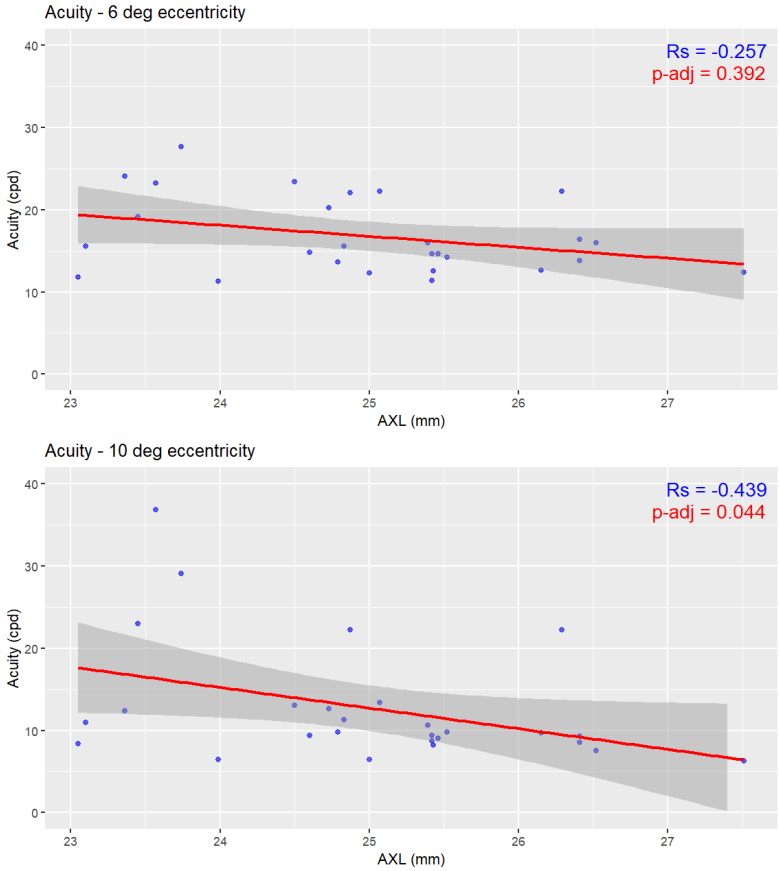

Figure 2.8. Spearman rank correlation of Acuity and axial length (AXL). At 10 deg, acuity was borderline significantly correlated with AXL (Rs = -0.439, p = 0.044). This relationship was not significant at 6 deg eccentricity (Rs = -0.257, p = 0.392). P-values are adjusted for two eccentricities using Bonferroni method and reported to three digits of precision.

b. Acuity

The Acuity of each subject represents the high spatial frequency cutoff of the CSF, which is associated with clinical measures of visual acuity. Using a one-way ANOVA, a significant difference was noted between acuity at 6 and 10 deg eccentricity (F = 5.69, p = 0.021), with higher Acuity at 6 deg (Figure 2.5, Table 2.1), as expected. At 10 deg eccentricity, a negative

correlation was present with AXL (Rs = -0.439, p = 0.044), which reached both the unconventional $\alpha < 0.10$ and the conventional cutoff for statistical significance ($\alpha < 0.05$).

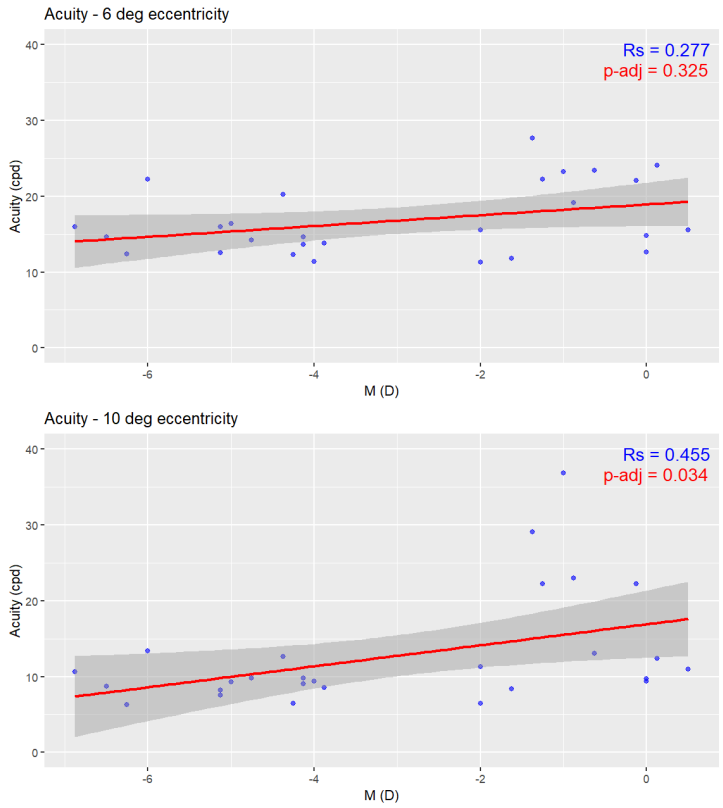

Figure 2.9. Spearman rank correlation of Acuity spherical equivalent refractive error (M) at 6 and 10 deg eccentricity. At 10 deg, acuity was statistically significantly correlated with M (Rs = 0.455, p = 0.034). This relationship was not significant at 6 deg eccentricity (Rs = 0.277, p = 0.325). P-values are adjusted for two eccentricities using Bonferroni method and reported to three digits of precision.

However, at 6 deg eccentricity, no relationship was observed with AXL (Rs = -0.257, p = 0.392) (Figure 2.8). As anticipated, promising results were noted for the secondary analysis with M. With M, a positive correlation was noted at 10 deg (Rs = 0.455, p = 0.034), but not at 6 deg eccentricity (Rs = 0.277, p = 0.325) (Figure 2.9). Therefore, we find that longer/more myopic eyes have lower high spatial frequency cutoffs, this is not unexpected since greater photoreceptor

spacing is anticipated [62]. What is interesting is the dichotomy between 6 and 10 deg eccentricity, which may be due to a differential rate of stretching in the 10 deg compared to the 6 deg region.

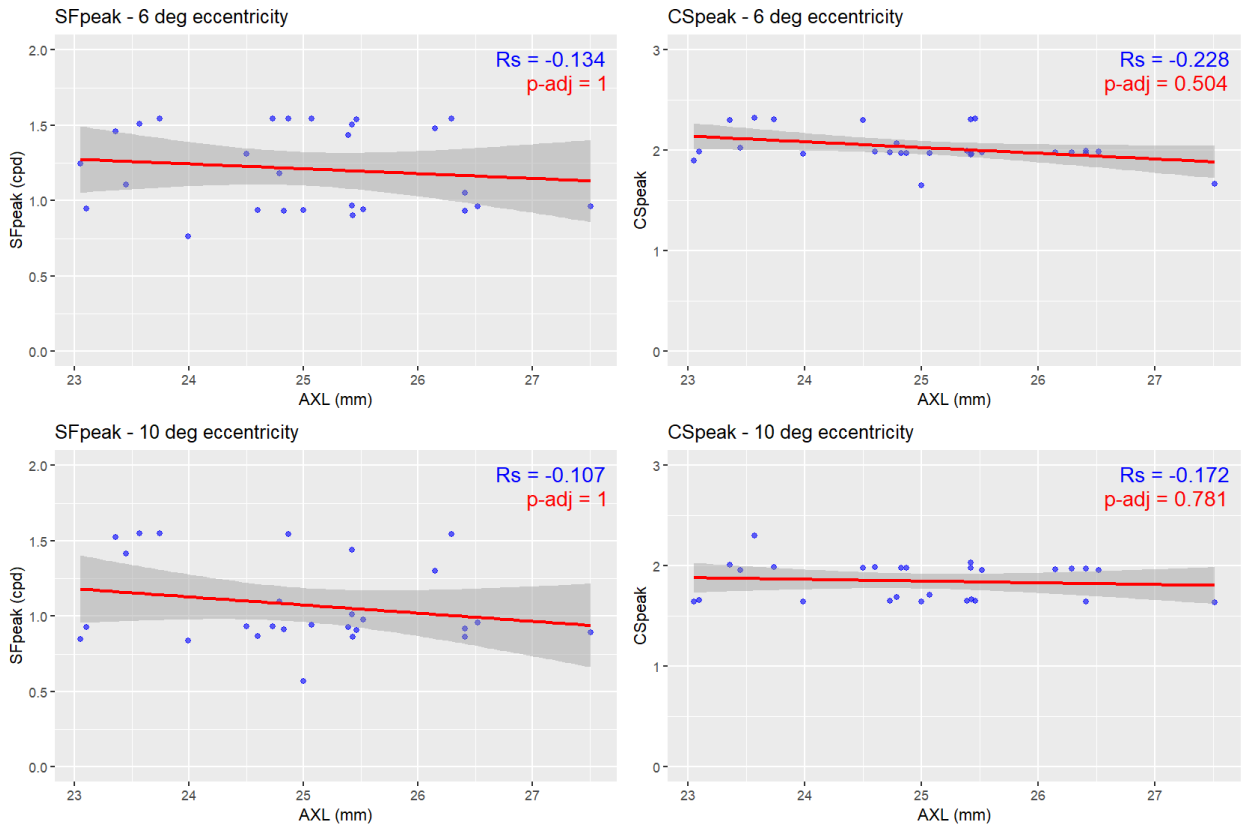

Figure 2.10. Spearman rank correlation of the location of the peak of the CSF curve (SFpeak and CSpeak) and axial length (AXL). No significant relationships were noted between either SFpeak or CSpeak and AXL. P-values are adjusted for two eccentricities using Bonferroni method and reported to three digits of precision.

c. Location of the CSF Peak

The location of the CSF peak was determined both as the spatial frequency (SFpeak) and contrast sensitivity (CSpeak) at the peak. On one-way ANOVA, no significant difference was identified between SFpeak group means at 6 and 10 deg eccentricity ($F = 3.18$, $p = 0.081$). However, a statistically significant difference was noted between eccentricities for CSpeak ($F = 13.5$, $p < 0.001$), where the CSpeak was higher at 6 deg than at 10 deg (Figure 2.5, Table 2.1).

No correlations met the unconventional $\alpha < 0.1$ between AXL and either SFpeak or CSpeak at either 6 or 10 deg eccentricity (Figure 2.10). At 10 deg eccentricity, CSpeak showed a weak positive correlation with M (Rs = 0.386, p = 0.094) (Figure 2.11), suggesting that the peak contrast sensitivity of myopes may be lower than emmetropes in the periphery. This is to be expected based on previous work that suggests a relationship between contrast sensitivity and axial length/refractive error especially when attention is attracted to a central location [62,63].

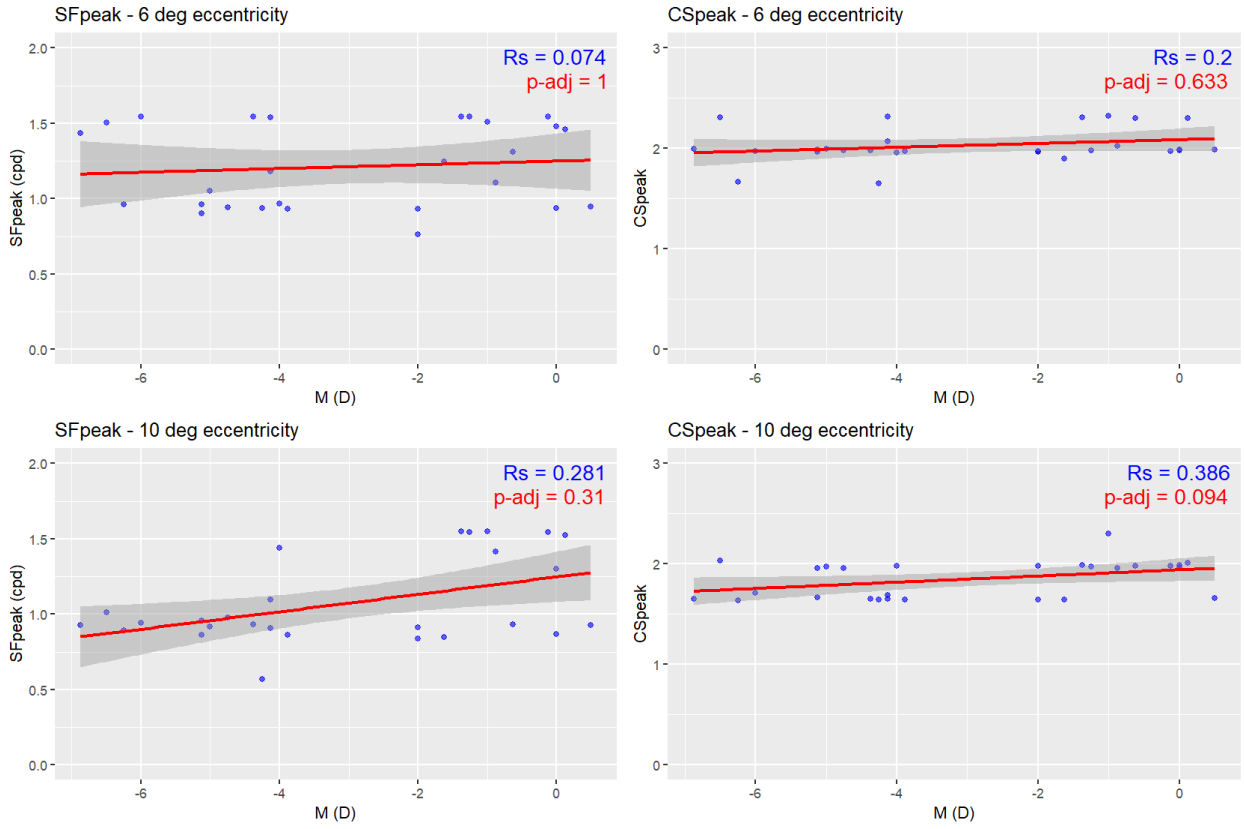

Figure 2.11. Spearman rank correlation of the location of the peak of the CSF curve (SFpeak and CSpeak) and spherical equivalent refractive error (M). No significant relationships were noted between either SFpeak or CSpeak and M. P-values are adjusted for two eccentricities using Bonferroni method and reported to three digits of precision.

3. Experiment 2: Threshold versus Contrast (TvC) Function

3.1 TvC Methods

This experiment aimed at elucidating the effect of lateral inhibition on the subject's visual function. This was achieved by measuring a threshold versus contrast (TvC) function with surround contrast as the pedestal value. For this, we modulated the contrast of a surround to elucidate the effect of surround contrast on the perception of a central sine-wave luminance grating. For this series of experiments, the presentation of the target and surround were controlled using circular polarization to produce either monocular or dichoptic viewing. Both eyes were open during testing. Under monocular conditions, the target stimulus and surround were presented to the right eye only. Under dichoptic conditions, the target stimulus was presented to the right eye, while the surround was presented to the left eye. This was used to differentiate effects at the retinal versus the cortical processing level. Subjects wore appropriate spectacle correction, as indicated above.

For this series of experiments, the TvC was measured with adaptive thresholding for each subject using the AIM protocol for the foveal location and the QuestPlus protocol for peripheral locations. The threshold versus contrast (TvC) function was measured at the same three retinal locations where CSF was obtained: 0-4, 4-8 and 8-12 deg eccentricity from the fovea. Targets were sine-wave luminance gratings with randomly varying contrast (range = 0.0125 - 0.40) and constant spatial frequency (4 cpd). Targets were circular, spanning 4 deg visual angle diameter and having a Gaussian profile (fading toward the edges). The surround of each stimulus contained isotropic noise with a given contrast level (pedestal contrast) and a dominant spatial frequency matching that of the central grating.

At the fovea (0 deg), the stimuli were presented in a grid pattern with subjects able to look freely at each stimulus (similar to the CSF experiment previously described). The surround was an annular ring around each target (Figure 3.1). Stimuli were tested at 5 surround contrast levels (4%, 8%, 16%, 32%, 64%). Subjects were asked to select the orientation of the stimulus using a mouse. Once again, the angular error was determined by the difference between the selected and actual orientations of the stimuli.

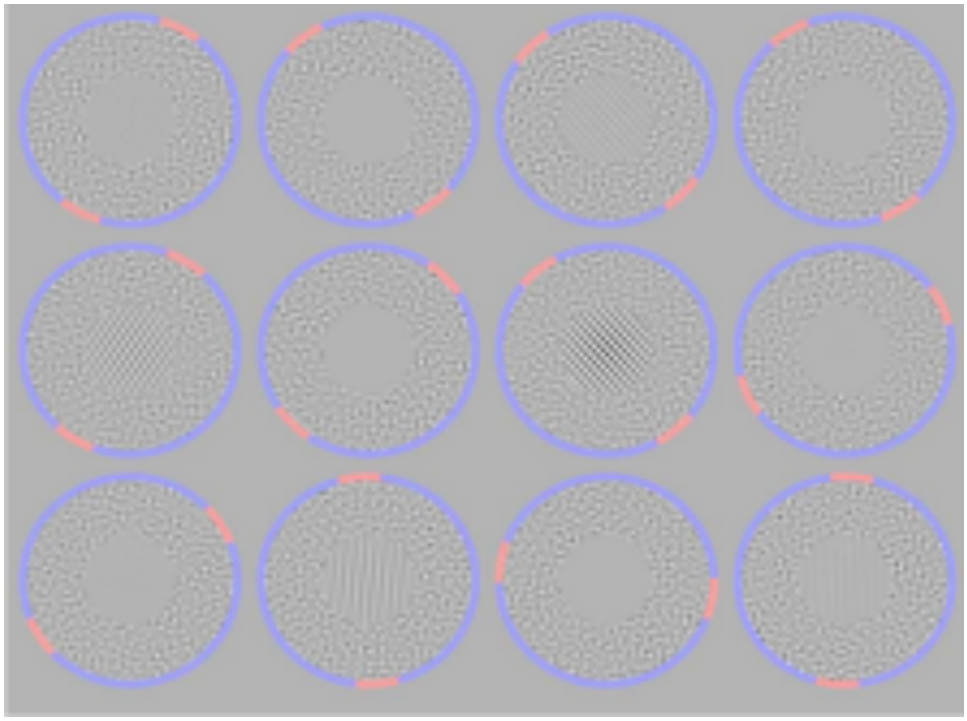

Figure 3.1. Representative stimulus for foveal (0 deg) center-surround antagonism experiments. Upon selecting orientation of stimulus, pink areas appear to indicate position chosen by subject. In this example, the subject has already selected the orientation of all stimuli. Central sine wave grating is surrounded by isotropic noise of given contrast.

In the periphery, the entire ring for each eccentricity region (4-8 or 8-12 deg) contained the appropriate isotropic noise for the stimulus. The ring of noise contained 8 holes, with the stimulus appearing in one of the 8 locations with each trial, creating an eight-alternative forced choice (8AFC) paradigm (Figure 3.2). Each stimulus was presented individually, appearing for

100 ms and only when the subject was looking at the central fixation point. Subjects were asked to identify the location where the target appeared when able. Experiments were conducted under photopic conditions. A curve was fitted to the data at each background contrast level and from this function, the neural Threshold contrast versus response (TvC) function was estimated [29].

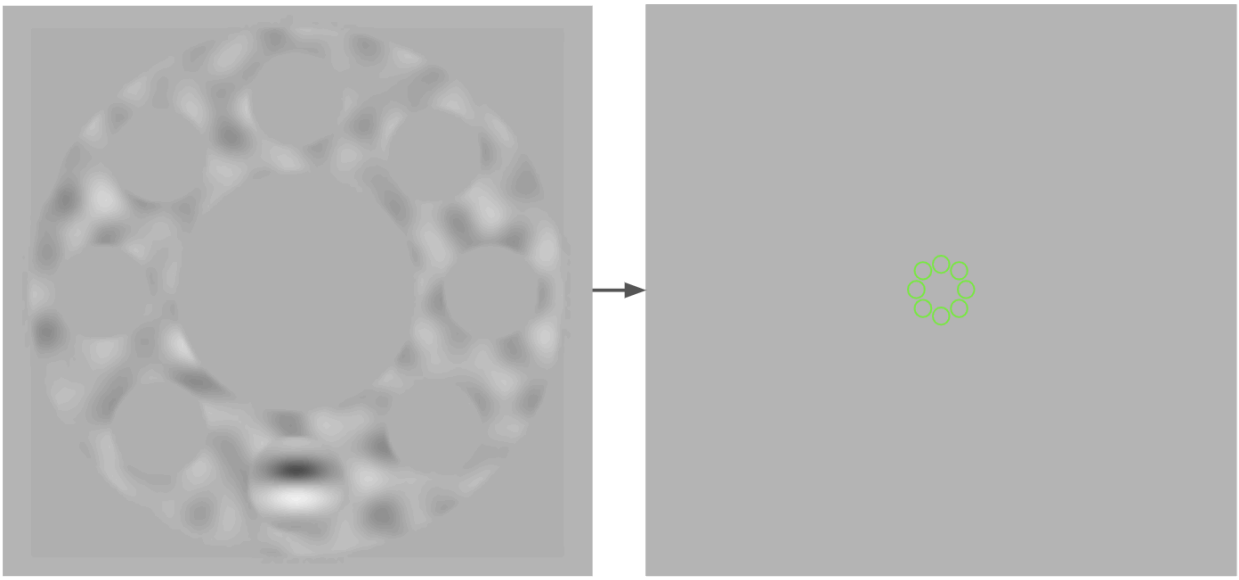

Figure 3.2. Representative stimulus for peripheral threshold versus contrast (TvC) function experiment tested at 6 deg eccentricity. The left image represents the moment when the stimulus is being actively presented. A ring of isotropic noise is presented in a ring surrounding fixation spanning either 4-8 deg (shown here) or 8-12 deg eccentricity. The 8 circles are cut outs within the noise, representing possible locations where the stimulus may be presented; only one of these locations contains a Gaussian sine-wave grating (in the inferior location in the example shown here). After a brief (100 ms) stimulus presentation, the response ring appears centrally with the 8 possible locations surrounding fixation (right image). Once the subject selects from the response ring, the next stimulus is presented, and the cycle repeats.

3.2 TvC Results

The Threshold versus Contrast Function (TvC) was measured (1) monocularly with both the target and the surround presented to in the right eye only and (2) dichoptically with the target presented to the right eye only and the surround presented to the left eye only. The presentation of target and stimulus was controlled through circular polarization. At each peripheral

eccentricity, Threshold versus Contrast (TvC) curves were calculated to achieve the best estimate of the true curve based on the data obtained (Figures 3.3 and 3.4).

The TvC function evaluates the contrast threshold to a given stimulus in the presence of different levels of a pedestal variable. In this case, the pedestal variable is the contrast of the surrounding isotropic noise and the target is a sine wave grating. Spatial frequency of the target and surround are equal and held constant. The resultant curve is a dipper function. If the surrounding contrast facilitates perception of the target, the curve will have a greater magnitude "dip" or minimum relative to baseline; if there is no effect, the curve should be relatively flat. Curve fits are approximated by the following equation:

$$\Delta c = \sqrt{(1 + 1/\psi)(\sigma_e^2 + \sigma_i^2)} \; - \; \sigma_e^2$$

In this curve fit, the contrast threshold (Δc) is the dependent variable, which is modulated the level of surround contrast (σ_e). Two fit parameters are necessary to complete the equation: (1) the sensitivity of the visual system to changes in contrast (Ψ), from this point on referred to as Psi; and (2) the intrinsic contrast threshold of the visual system (σ_i), from this point on referred to as intrinsic noise (IN) [64]. The intrinsic noise (IN) accounts for the initial plateau and decrease in the TvC dipper function, while Psi governs the rising arm of the function in accordance with Weber's Law [64].

From these curves, the following data points were extracted: (1) area under the TvC curve (AUTVC), (2) intrinsic noise (IN) of the visual system, (3) sensitivity to changes in contrast (Psi), (4) pedestal contrast at the function's minimum (MinPedes), (5) contrast threshold at the function's minimum (MinThresh). These are correlated with AXL with Spearman rank

analysis as the primary outcome of the study. For completeness, results are also correlated with M. Two-way Robust ANOVA (based on Wilcox's method) was performed to assess differences between group means at 6 versus 10 deg eccentricity and under monocular versus dichoptic conditions (Figure 3.5). The Robust ANOVA was chosen in this case due to unequal variances among the data set. For all graphs related to this data set, monocular findings are presented on the left and dichoptic on the right.

After selecting complete data sets and removing outliers, 24 subjects were included in the analysis of the TvC function. For each outcome, p-values are adjusted using the Bonferroni method to account for measurement at two eccentricities (6 and 10 deg). As noted in section 1.6, the unconventional alpha cutoff of 0.2 was determined through power analysis utilizing the largest effect size of a TvC outcome correlation with AXL (primary outcome). Of outcomes related to TvC, the greatest effect size was seen between AXL and MinThresh at 10 deg under dichoptic testing conditions (Rs = -0.432, Figure 4.22). Using this cutoff, we identify correlations that may merit further research and have interesting implications as they pertain to the role of lateral interactions in myopia.

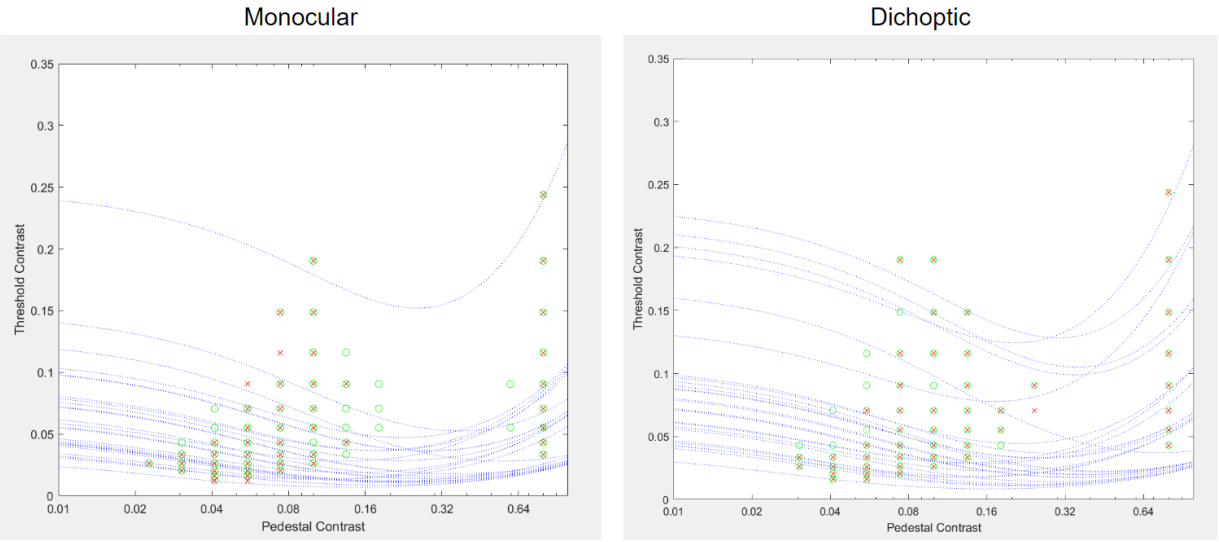

Figure 3.3. Threshold versus Contrast (TvC) curve fits for all subjects measured at 6 deg eccentricity in the peripheral retina. The threshold contrast detected by the subject was plotted as a function of pedestal contrast. The left image depicts monocular results, while the right image depicts dichoptic results. Both axes are plotted in logarithmic notation. Green circles represent data points where the subjects correctly identified the stimulus location, whereas red Xs represent data points where subjects incorrectly identified the location.

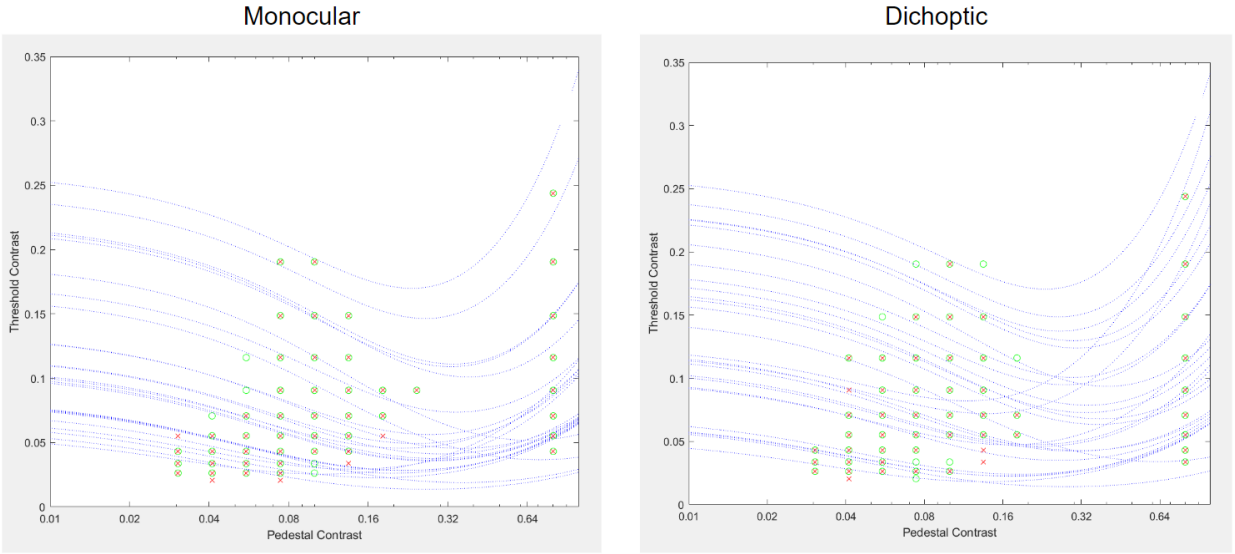

Figure 3.4. Threshold versus Contrast (TvC) curve fits for all subjects measured at 10 deg eccentricity in the peripheral retina. The threshold contrast detected by the subject was plotted as a function of pedestal contrast. The left image depicts monocular results, while the right image depicts dichoptic results. Both axes are plotted in logarithmic notation. Green circles represent data points where the subjects correctly identified the stimulus location, whereas red Xs represent data points where subjects incorrectly identified the location.

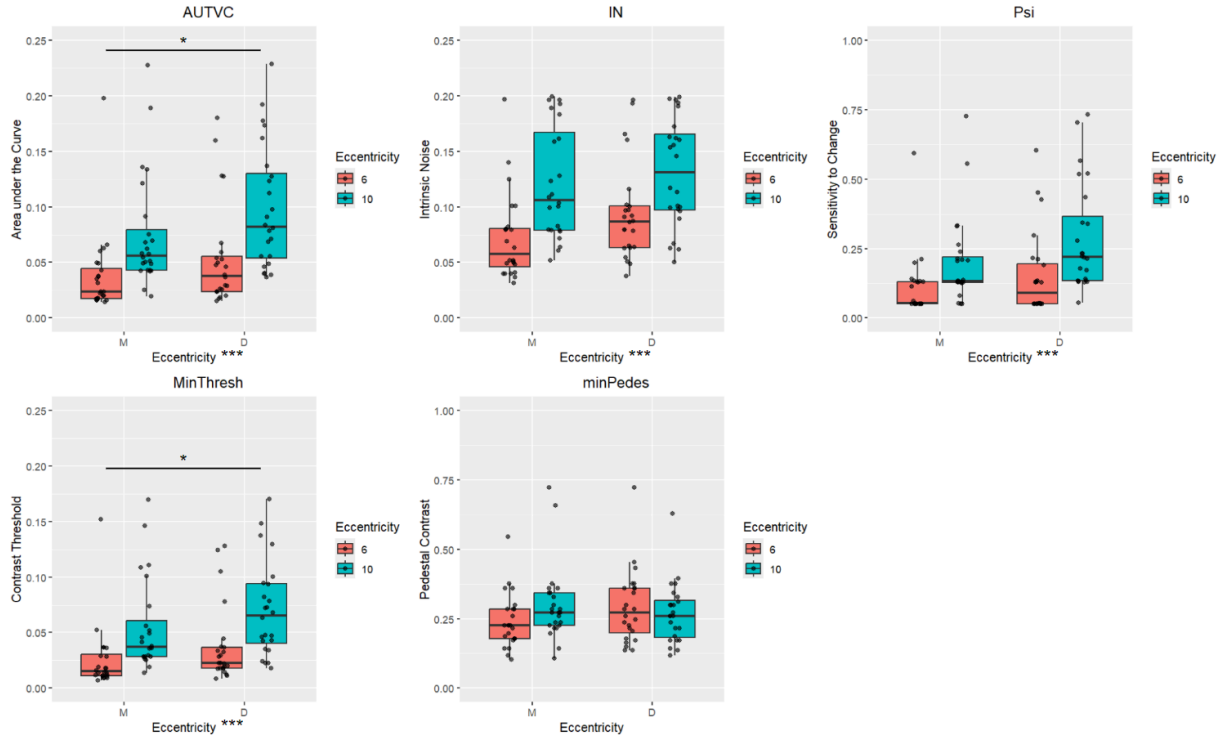

Figure 3.5. Comparison of TvC outcomes at 6 and 10 deg eccentricity and under monocular (M) and Dichoptic (D) testing conditions using Two-way Robust ANOVA (based on Wilcox's method). Two-way Robust ANOVA of outcomes related to the TvC function showed a statistically significant difference between eccentricities for AUTVC (Statistic = 21.320, $p < 0.001$), IN (Statistic = 22.562, $p < 0.001$), Psi (Statistic = 16.083, $p < 0.001$), and MinThresh (Statistic = 23.718, $p < 0.001$). In all cases, the results were higher when tested at 10 deg than when tested at 6 deg. No statistically significant difference between eccentricities was noted for minPedes (Statistic = 0.728, $p = 0.398$). Statistically significant differences between monocular and dichoptic conditions were noted for AUTVC (Statistic = 4.701, $p = 0.037$) and MinThresh (Statistic = 4.411, $p = 0.042$) where results were higher under dichoptic conditions than under monocular conditions. No significant differences between conditions were noted for IN (Statistic = 3.095, $p = 0.086$), Psi (Statistic = 3.516, $p = 0.071$), or minPedes (Statistic = 0.489, $p = 0.488$). Significance levels are as follows *** $p < 0.001$, ** $p < 0.01$,
* $p < 0.05$. P-values are reported to three digits of precision.

Table 3.1. Summary statistics for TvC outcomes separated by eccentricity and monocular/dichoptic testing conditions. All parameters are reported with 3 digits of precision.

Variable	Eccentricity	Monocular.Mean	Monocular.SD	Monocular.Min	Monocular.Max	Dichoptic.Mean	Dichoptic.SD	Dichoptic.Min	Dichoptic.Max
AUTVC	6	0.038	0.038	0.014	0.198	0.054	0.047	0.016	0.180
AUTVC	10	0.075	0.051	0.019	0.228	0.099	0.055	0.037	0.229
IN	6	0.072	0.039	0.031	0.197	0.094	0.044	0.038	0.196
IN	10	0.121	0.050	0.052	0.199	0.131	0.049	0.050	0.199
Psi	6	0.110	0.115	0.050	0.594	0.152	0.151	0.050	0.603
Psi	10	0.201	0.158	0.051	0.726	0.287	0.193	0.054	0.732
MinThresh	6	0.025	0.030	0.007	0.152	0.038	0.035	0.008	0.128
MinThresh	10	0.055	0.042	0.014	0.170	0.071	0.043	0.018	0.171
minPedes	6	0.240	0.099	0.102	0.546	0.291	0.132	0.135	0.722
minPedes	10	0.301	0.137	0.107	0.722	0.269	0.110	0.118	0.628

a. Area Under the Curve (AUTVC)

The area under the entire TVC curve was calculated for each subject and plotted against AXL (Figure 3.6) and M (Figure 3.7). Two-way Robust ANOVA showed a statistically significant difference in AUTVC between eccentricities (Statistic = 21.320, $p < 0.001$) and between conditions (Statistic = 4.701, $p = 0.037$). Both monocularly and dichoptically, results were higher when tested at 10 deg than when tested at 6 deg eccentricity (Figure 3.5, Table 3.1). Additionally, the area under the curve was higher under dichoptic conditions than under monocular conditions. A lower overall contrast threshold at further eccentricities into the periphery is expected and coincides with the results of the CSF experiment where higher overall contrast sensitivity was noted at 6 deg than at 10 deg eccentricity [62,63,65].

No significant relationships were noted between AUTVC and AXL at either eccentricity under monocular (6 deg Rs = 0.046, $p = 1.000$; 10 deg Rs = 0.178, $p = 0.811$) or dichoptic (6 deg Rs = 0.391, $p = 0.188$; 10 deg Rs = 0.237, $p = 0.529$) testing conditions (Figure 3.6). Based on our unconventional alpha cutoff of 0.2, a potentially interesting relationship was identified

between AUTVC and AXL when tested under dichoptic conditions at 6 deg eccentricity (Rs = 0.391, p = 0.188). Similarly, no significant relationships were noted between AUTVC and M at either eccentricity under monocular (6 deg Rs = -0.347, p = 0.193; 10 deg Rs = -0.179, p = 0.806) or dichoptic (6 deg Rs = -0.335, p = 0.219; 10 deg Rs = -0.249, p = 0.480) conditions (Figure 3.7). However, a potentially interesting relationship is identified between AUTVC and M when tested under monocular conditions at 6 deg. Both identified relationships are noted at 6 deg eccentricity. In the absence of a pattern in monocular/dichoptic testing conditions or concordance between M and AXL correlations, these weak associations become less convincing.

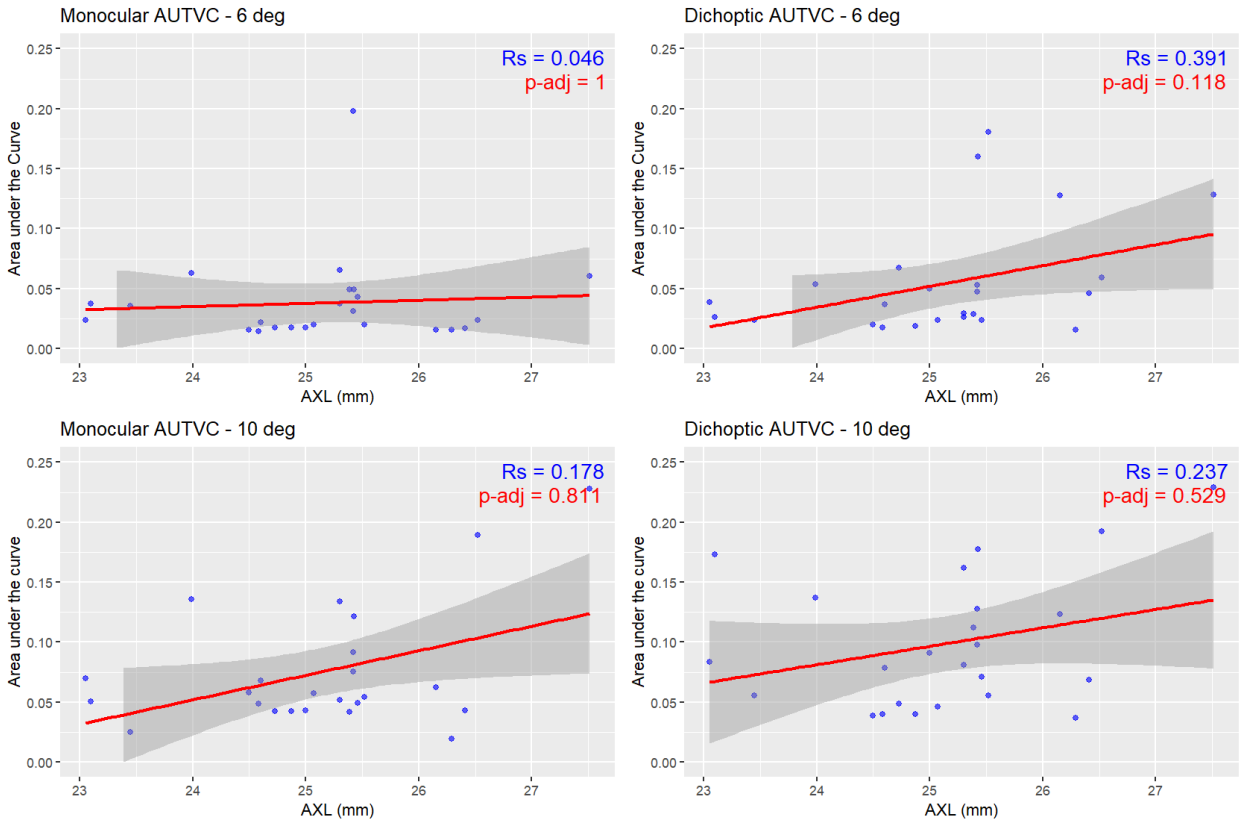

Figure 3.6. Spearman rank correlation of area under the Threshold versus Contrast (TvC) curve and axial length (AXL). No statistically significant correlations were found at either eccentricity or testing condition. P-values are adjusted for two eccentricities using Bonferroni method and reported to three digits of precision.

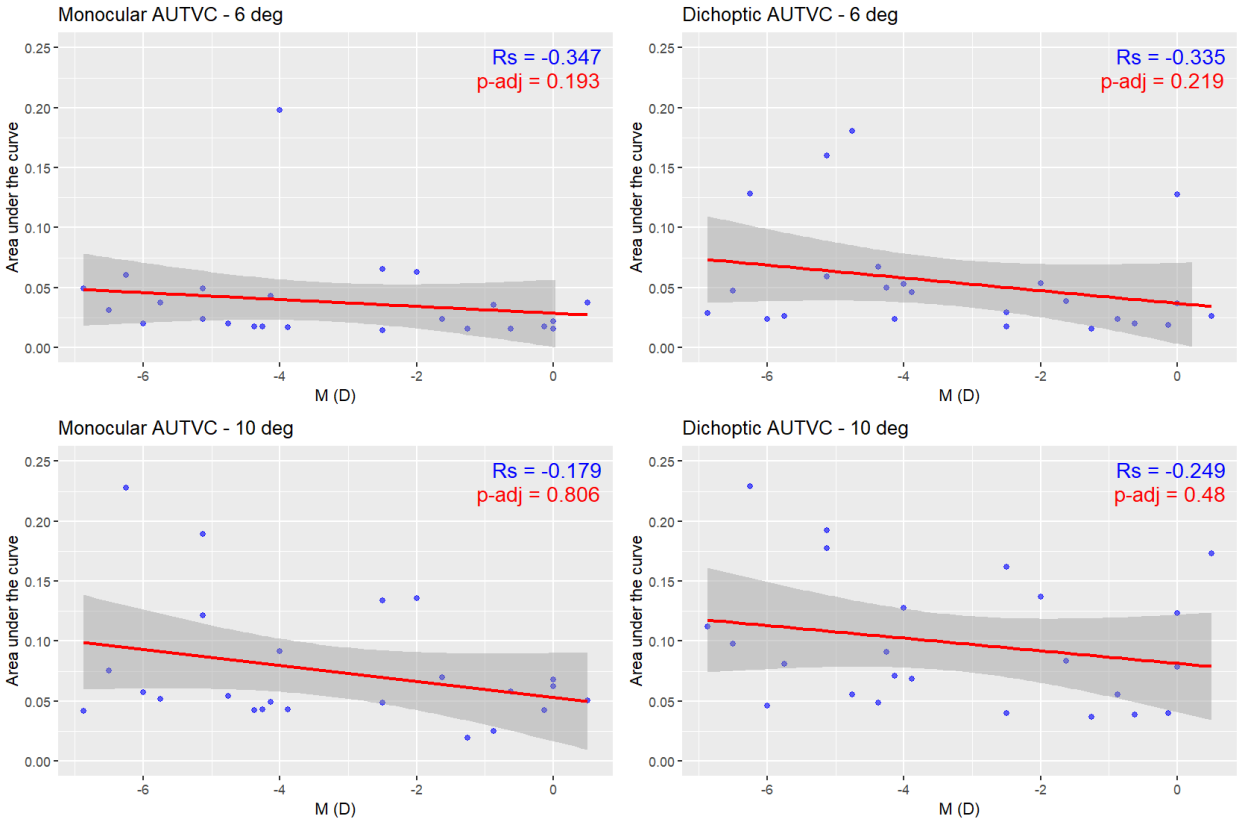

Figure 3.7. Spearman rank correlation of area under the Threshold versus Contrast (TvC) curve and spherical equivalent refractive error (M). No statistically significant correlations were found at either eccentricity or testing condition. P-values are adjusted for two eccentricities using Bonferroni method and reported to three digits of precision.

b. Intrinsic Noise (IN)

The Intrinsic Noise (IN) of the visual system represents the contrast threshold when no surrounding stimulation is present. The IN of the visual system is due to both optical and neural components of the visual system. In order to detect contrast in the visual system, the subject's internal processing must take this intrinsic contrast threshold into account. The intrinsic contrast threshold is responsible for the initial dip in the TvC function, while the increase following the minimum is subject to Weber's Law (see section c below) [64]. This was calculated and plotted against AXL (Figure 3.8) and M (Figure 3.9).

Two-way Robust ANOVA of outcomes related to the TvC function showed a statistically significant difference in IN between eccentricities (Statistic = 22.562, $p < 0.001$) where results were higher when tested at 10 deg than when tested at 6 deg eccentricity (Figure 3.5, Table 3.1), indicating a higher intrinsic noise at 10 deg than at 6 deg. This is not unexpected, since the visual system is weighted toward increased organization near the fovea [66]. There was no significant difference between monocular/dichoptic conditions.

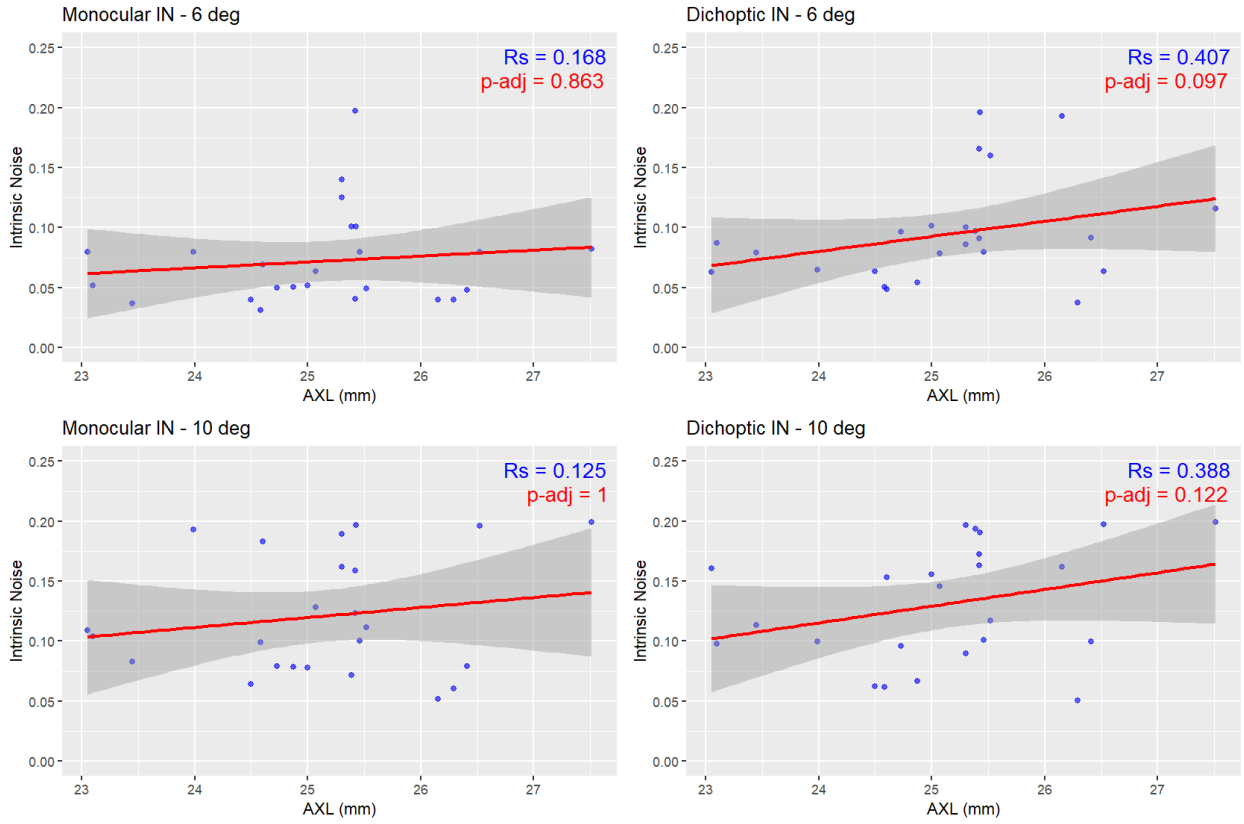

Figure 3.8. Spearman rank correlation of Intrinsic Noise (IN) and axial length (AXL). No statistically significant relationships were noted under monocular or dichoptic conditions at either eccentricity. P-values are adjusted for two eccentricities using Bonferroni method and reported to three digits of precision.

There were no statistically significant relationships found between IN and AXL under monocular (6 deg Rs = 0.168, p = 0.863; 10 deg Rs = 0.125, p = 1.000). However, under dichoptic testing conditions, the relationship between IN and AXL showed a promising positive

correlation at both 6 (Rs = 0.407, p = 0.097) and 10 deg eccentricity (Rs = 0.388, p = 0.122) (Figure 3.8). This may indicate that longer eyes tend to have higher intrinsic noise than shorter eyes, an idea which has some nascent support in the psychophysical perceptual learning literature with myopes [67]. All relationships between IN and M also reached the unconventional alpha cutoff, which is not unexpected given the known correlation between AXL and M (Figure 1.1). For both monocular (6 deg Rs = -0.415, p = 0.087; 10 deg Rs = -0.366, p = 0.157) and dichoptic conditions (6 deg Rs = -0.390, p = 0.199) more myopic eyes had higher intrinsic noise (Figure 3.9).

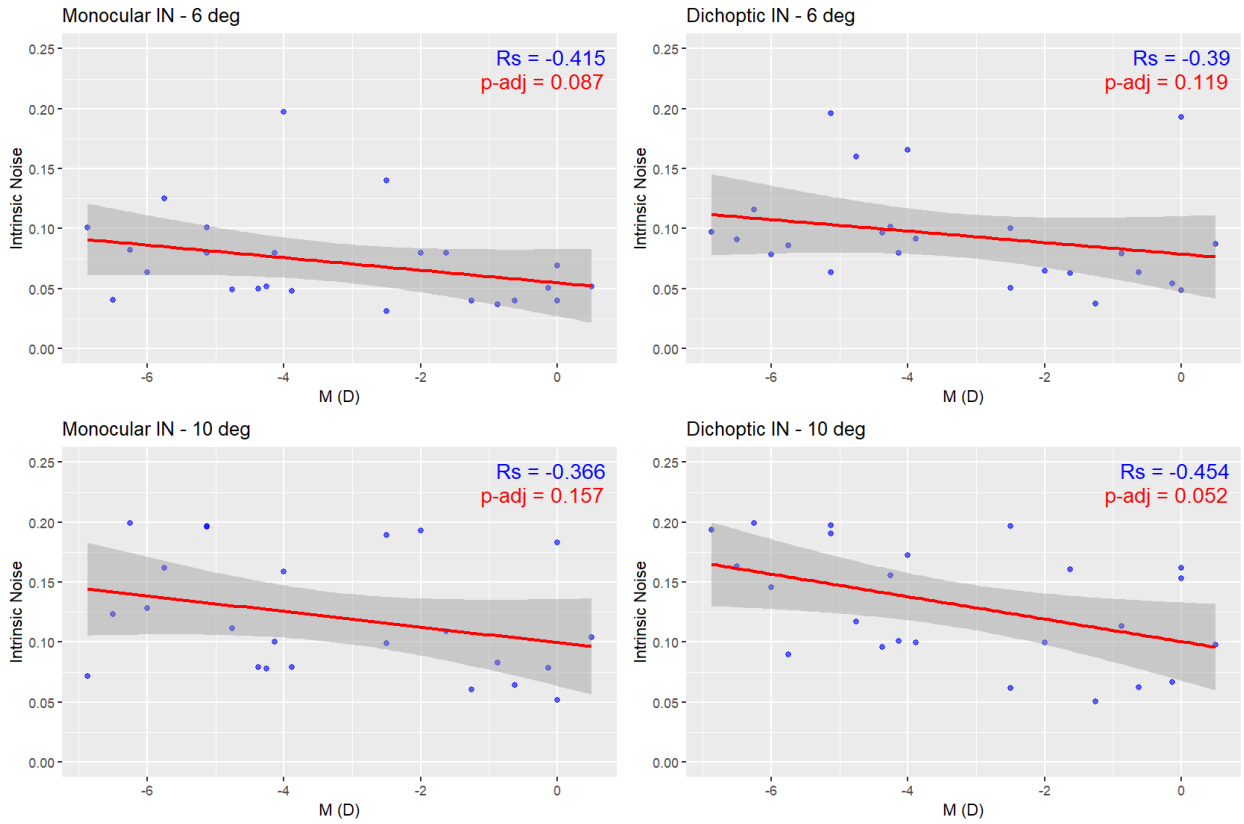

Figure 3.9. Spearman rank correlation of Intrinsic Noise (IN) and spherical equivalent refractive error (M). No statistically significant relationships were noted under monocular or dichoptic conditions at either eccentricity, though at 10 deg eccentricity the correlation between IN and M was approaching significance under dichoptic conditions (Rs = -0.454, p = 0.052). P-values are adjusted for two eccentricities using Bonferroni method and reported to three digits of precision.

c. Sensitivity to Changes/Differences in Blur (Psi)

The Psi measure is based on the Weber fraction, which helps us understand the just noticeable difference a person can perceive in contrast levels [64]. Two-way Robust ANOVA of outcomes related to the TvC function showed a statistically significant difference in Psi between eccentricities (Statistic = 16.083, $p < 0.001$) where Psi was higher when tested at 10 deg than at 6 deg, indicating that sensitivity to changes in surround contrast was higher at 10 deg. No significant differences were observed between monocular/dichoptic testing conditions (Figure 3.5, Table 3.1).

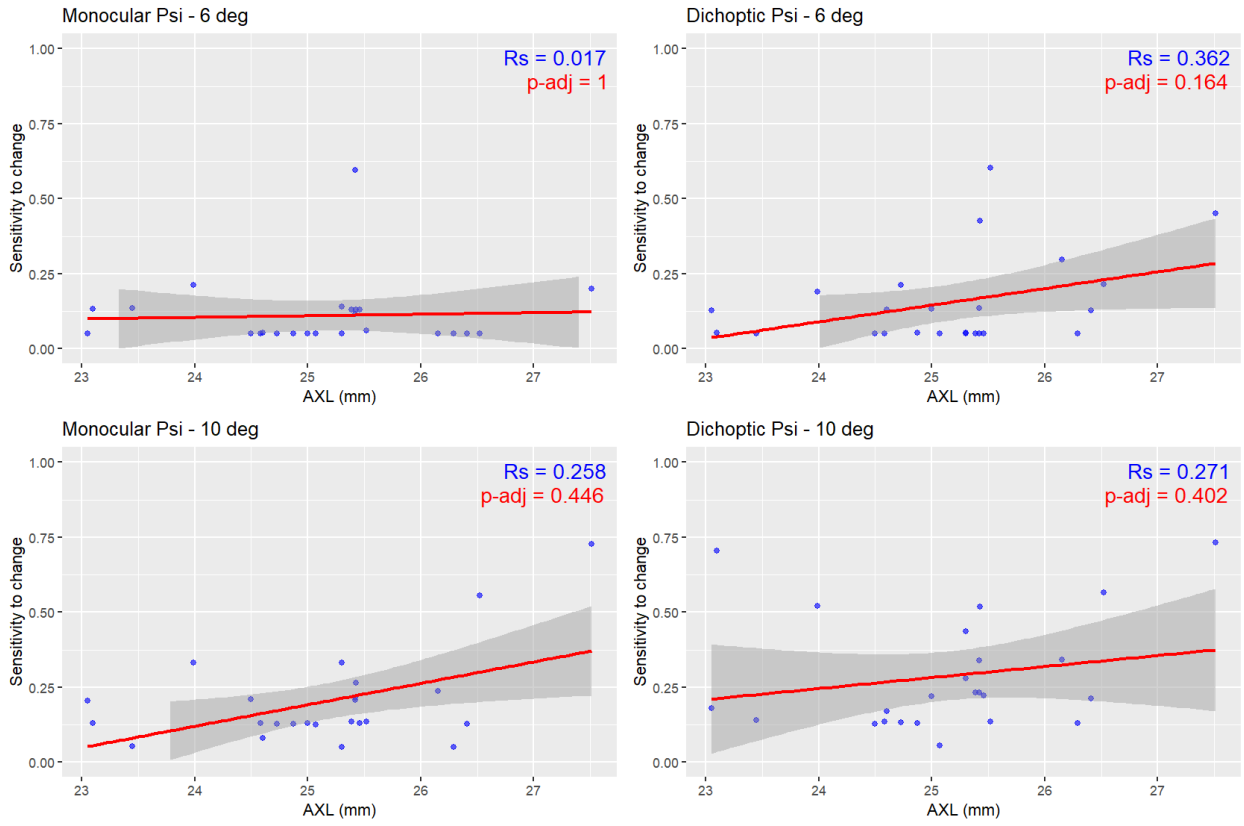

Figure 3.10. Spearman rank correlation of sensitivity to change in contrast (Psi) and axial length (AXL). No statistically significant relationships were found with AXL for either eccentric location or testing condition. P-values are adjusted for two eccentricities using Bonferroni method and reported to three digits of precision.

No statistically significant relationships were found between Psi and AXL under monocular (6 deg Rs = 0.017, p = 1.000; 10 deg Rs = 0.258, p = 0.446) testing conditions.Under dichoptic testing conditions, a weak positive correlation was noted between Psi and AXL at 6 deg (Rs = 0.362, p = 0.164), but not 10 deg (Rs = 0.271, p = 0.402) (Figure 3.10). No statistically significant correlations were found between Psi and M under either monocular (6 deg Rs = -0.179, p = 0.806; 10 deg Rs = -0.174, p = 0.830) or dichoptic (6 deg Rs = -0.240, p = 0.517; 10 deg Rs = -0.179, p = 0.806) testing conditions at either retinal eccentricity (Figure 3.11).

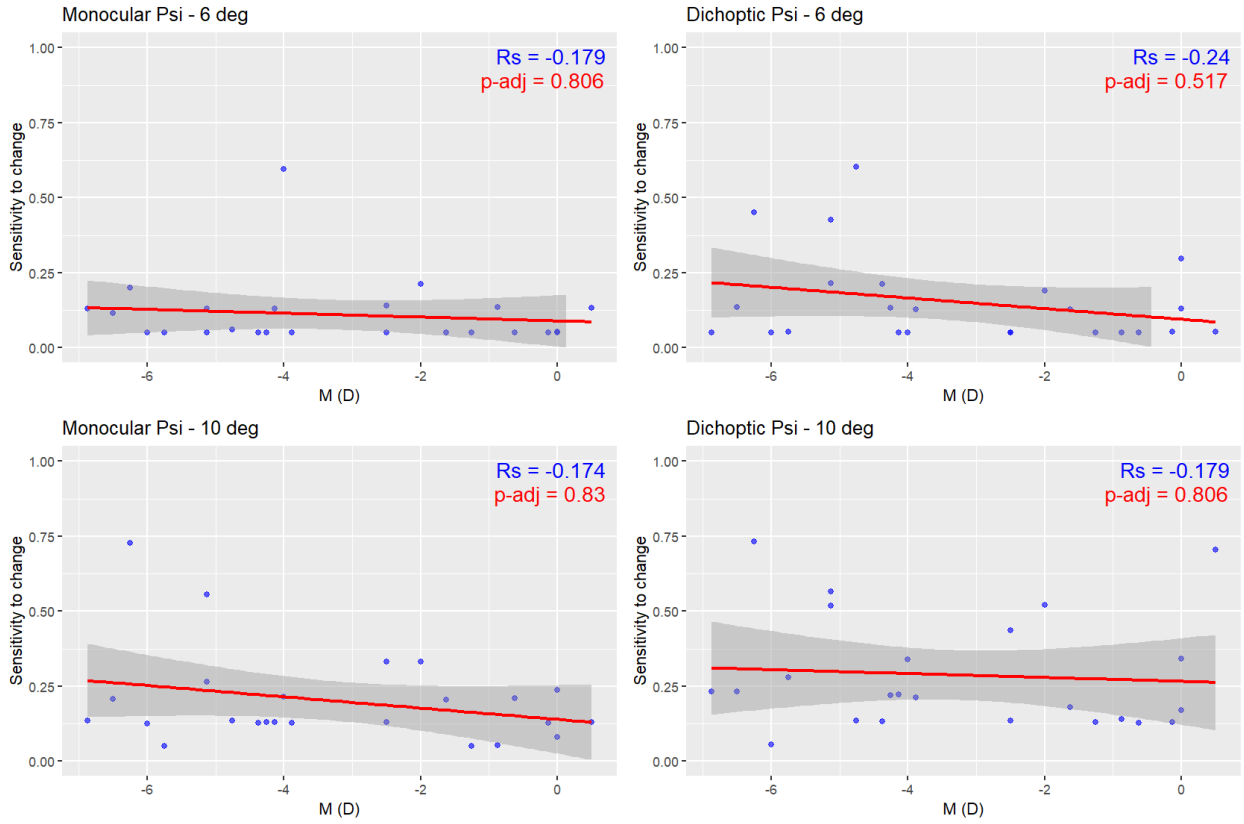

Figure 3.11. Spearman rank correlation of sensitivity to change in contrast (Psi) and spherical equivalent refractive error (M). No statistically significant relationships were found with M for either eccentric location or testing condition. P-values are adjusted for two eccentricities using Bonferroni method and reported to three digits of precision.

d. Location of TVC Function Minimum

The location of the Threshold versus Contrast Function's minimum was calculated with two parameters: the pedestal contrast at the function's minimum (MinPedes) and the contrast threshold at the function's minimum (MinThresh). Spearman Rank correlations were calculated for AXL (Figures 3.12 and 3.14), and M (Figures 3.13 and 3.15) for each of the two metrics.

Two-way Robust ANOVA of outcomes related to the TvC function showed a statistically significant difference in MinThresh between 6 and 10 deg eccentricity (Statistic = 23.718, $p < 0.001$) where the contrast threshold was higher when tested at 10 deg than at 6 deg. Again, a lower contrast threshold at 6 deg eccentricity corresponds with a higher contrast sensitivity at 6 deg than at 10 deg, which is the expected result. No significant differences were noted between monocular/dichoptic testing conditions. On two-way Robust ANOVA of minPedes, no statistically significant differences were found between eccentric locations (Statistic = 0.728, $p = 0.398$) or between monocular/dichoptic testing conditions (Statistic = 0.489, $p = 0.488$). This indicates that overall, eyes appear to have the lowest contrast threshold (highest contrast sensitivity) with a surround contrast of around 0.30 (Figure 3.5, Table 3.1).

No significant relationships were found between MinPedes and AXL at either 6 or 10 degrees eccentricity (Figure 3.12). Under dichoptic conditions, the relationship between minPedes and M met the unconventional $\alpha < 0.2$ at 10 deg (Rs = -0.36, $p = 0.168$), where more myopic eyes tended to reach a TvC minimum at lower pedestal contrast levels. However, no relationship was present under dichoptic conditions at 6 deg (Rs = -0.064, $p = 1.000$). No significant correlations were found between MinPedes and M under monocular testing

conditions (Figure 3.13). In the absence of an associated relationship between AXL and MinPedes or other patterns in the data set, these results are less convincing.

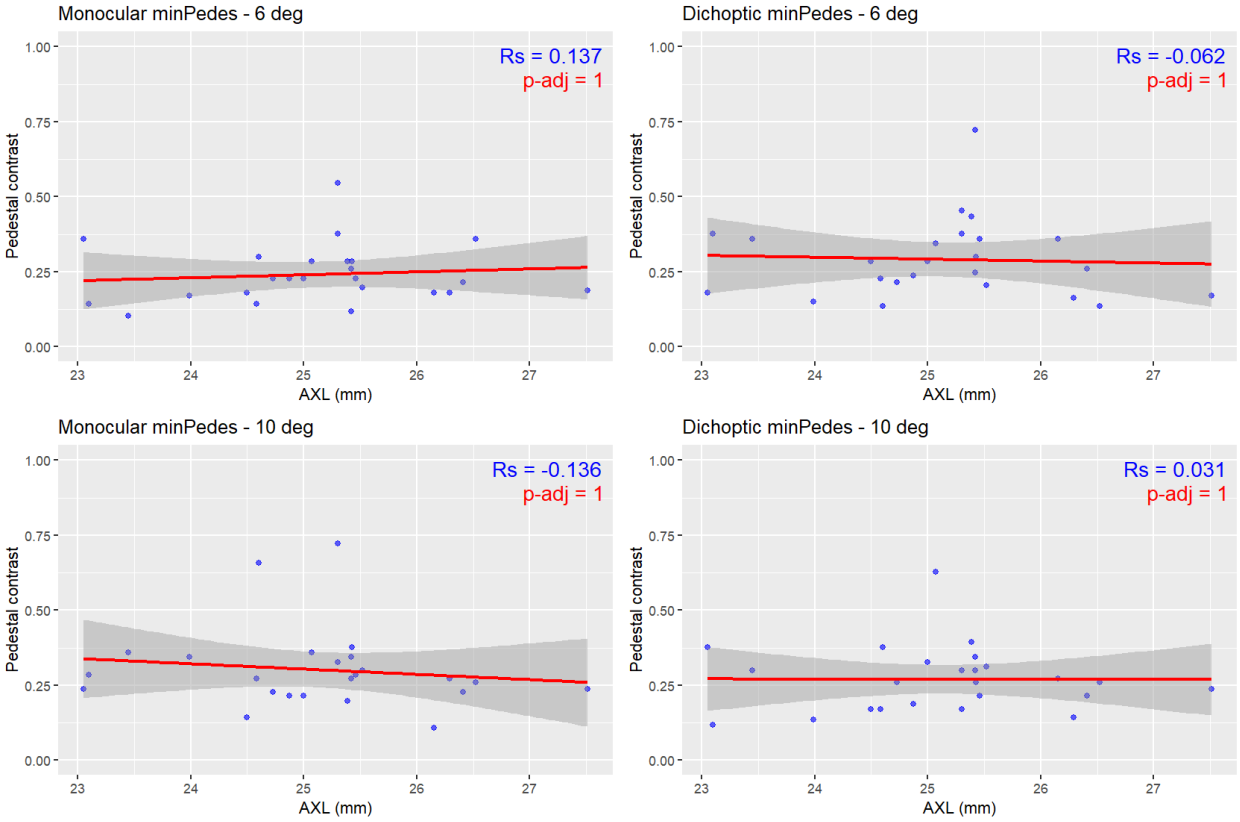

Figure 3.12. Spearman rank correlation of pedestal contrast at threshold versus contrast (TvC) function minimum (MinPedes) and axial length (AXL). No statistically significant relationships were found with AXL for either eccentric location or testing condition. P-values are adjusted for two eccentricities using the Bonferroni method and reported to three digits of precision.

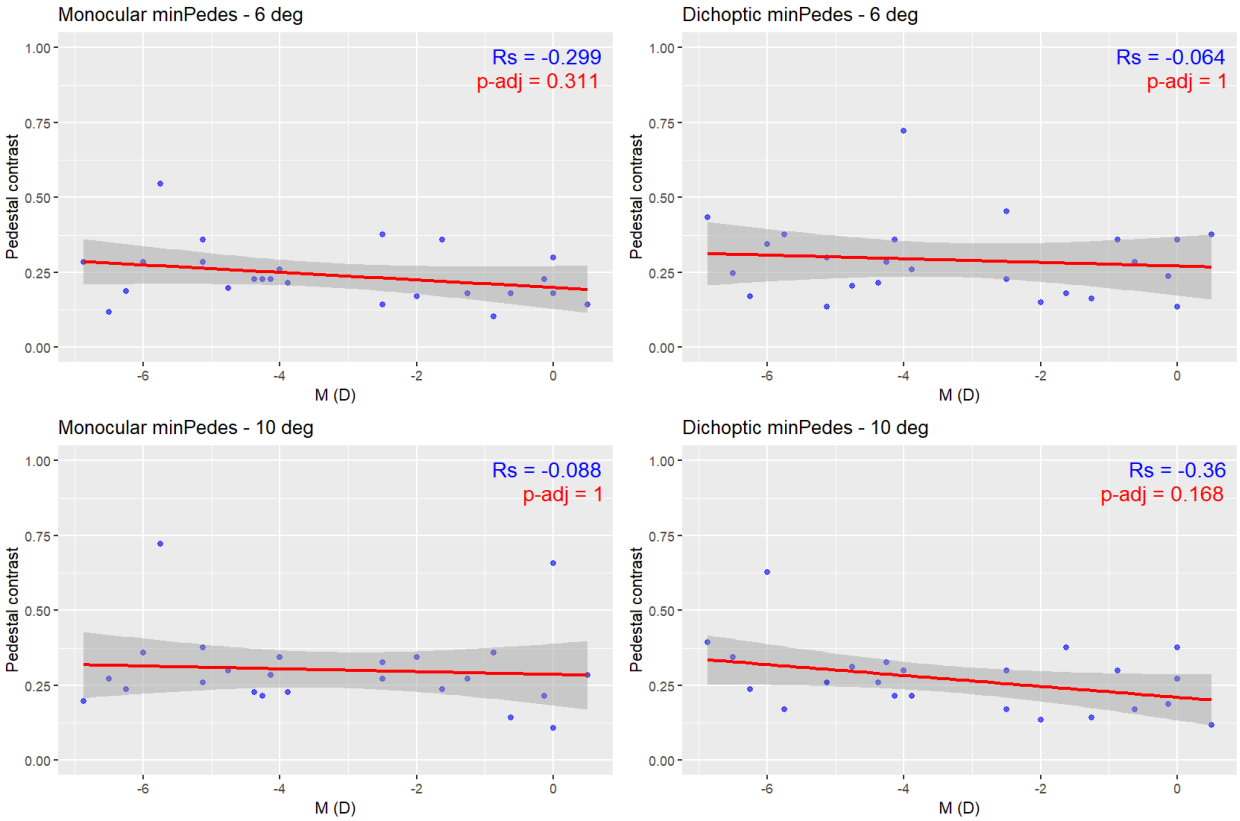

Figure 3.13. Spearman rank correlation of pedestal contrast at threshold versus contrast (TvC) function minimum (MinPedes) and spherical equivalent refractive error (M). No statistically significant relationships were found with M for either eccentric location or testing condition. P-values are adjusted for two eccentricities using the Bonferroni method and reported to three digits of precision.

No significant correlations were observed between MinThresh and AXL when tested under monocular conditions at either 6 or 10 degrees eccentricity. Under dichoptic conditions, weak positive correlations were noted between MinThresh and AXL at both 6 (Rs = 0.432, p = 0.07) and 10 deg (Rs = 0.348, p = 0.19) (Figure 3.14), where longer eyes had a higher contrast threshold at the function's minimum. At 6 deg eccentricity, weak negative correlations were noted between MinThresh and M under both monocular (Rs = -0.348, p = 0191) and dichoptic (Rs = -0.404, p = 0.100) testing conditions (Figure 3.15). No significant correlations were noted between MinThresh and M at 10 deg eccentricity for either testing condition (Figure 3.15). The trend toward longer/more myopic eyes having lower maximum contrast sensitivities is not

unexpected based on our understanding of photoreceptor spacing with increasing axial length [65]. However, the preponderance of promising data sets found under dichoptic conditions only raises questions about the origin of the pattern.

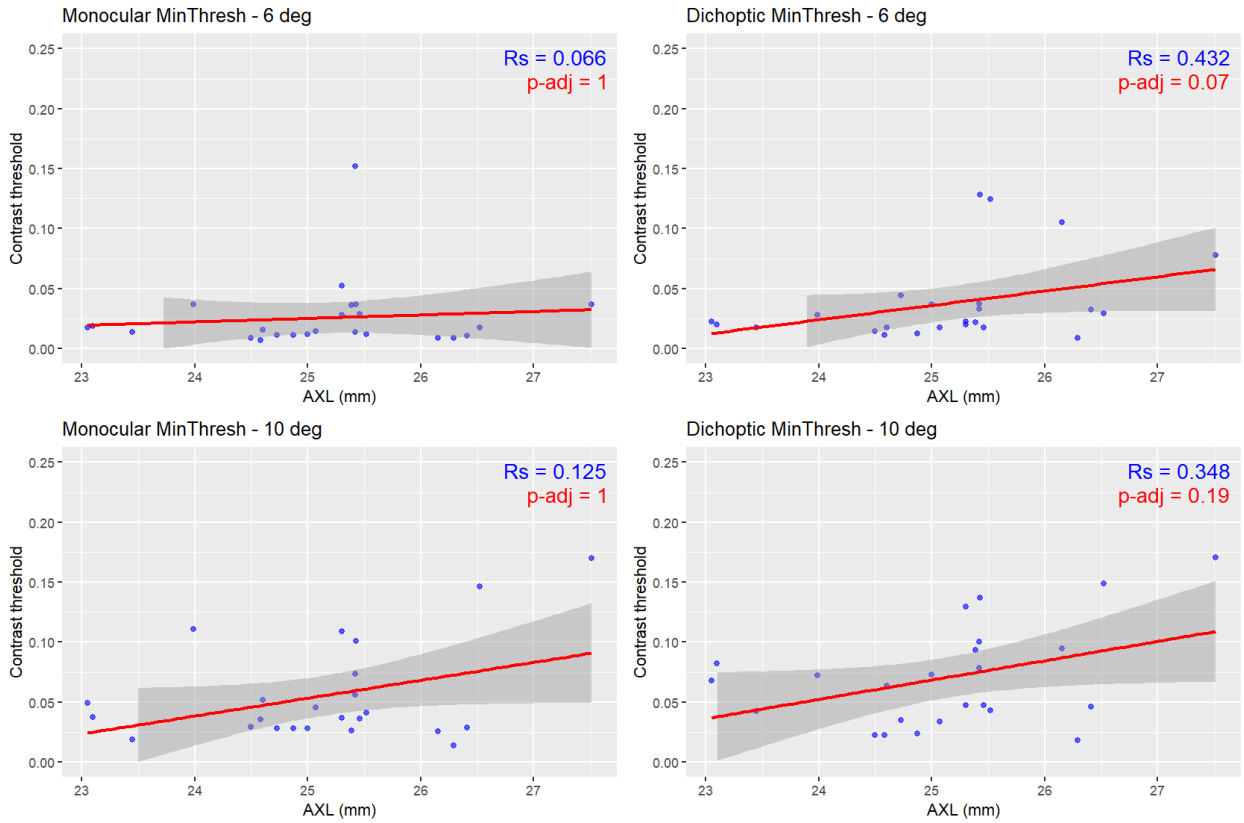

Figure 3.14. Spearman rank correlation of contrast threshold at threshold versus contrast (TvC) function minimum (MinThresh) and axial length (AXL). No statistically significant relationships were found between MinThresh and AXL for either eccentric location or testing condition. P-values are adjusted for two eccentricities using the Bonferroni method and reported to three digits of precision.

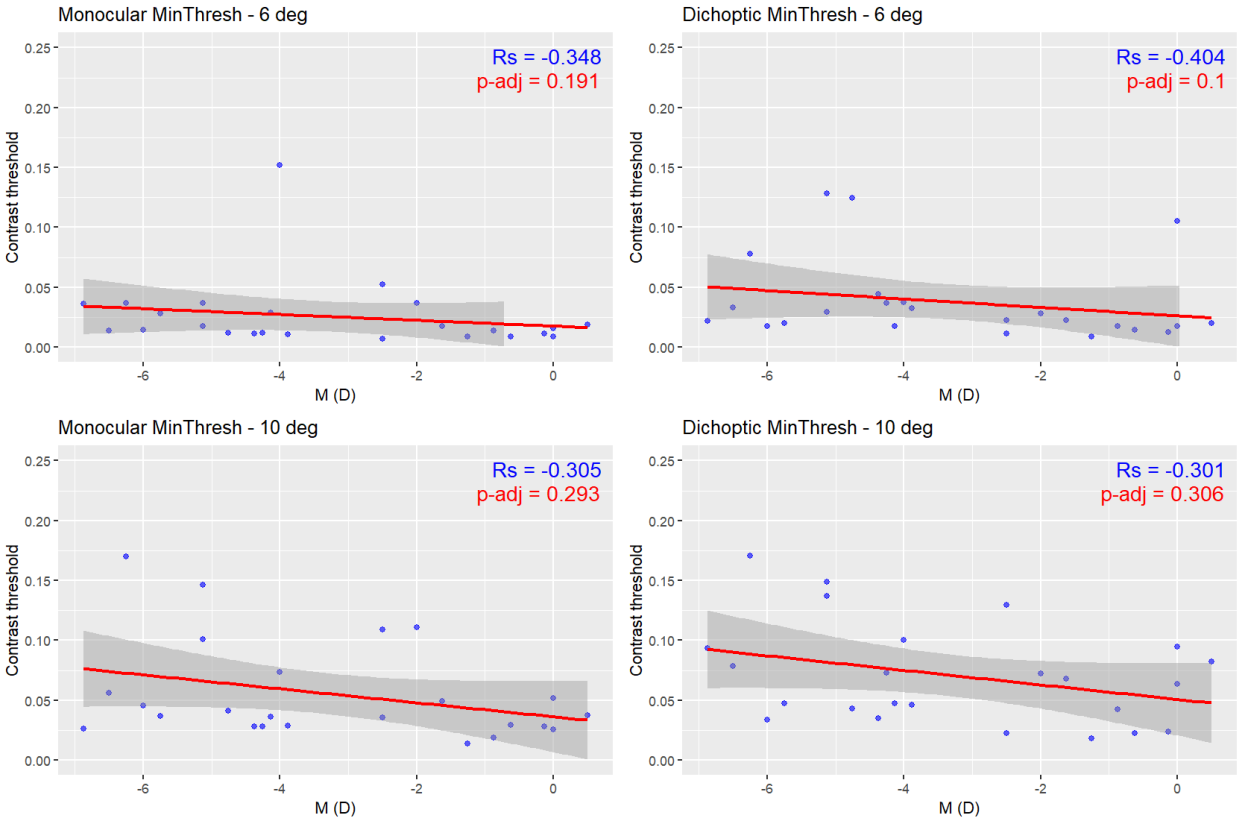

Figure 3.15. Spearman rank correlation of contrast threshold at threshold versus contrast (TvC) function minimum (MinThresh) and spherical equivalent refractive error (M). No statistically significant relationships were found between MinThresh and M at either eccentric location or testing condition. P-values are adjusted for two eccentricities using the Bonferroni method and reported to three digits of precision.

4. Experiment 3: Electrophysiology

4.1 Electrophysiological Methods

a. Surround Contrast vs ERG/VEP Response

To investigate lateral processing within the retina, a custom stimulus was designed to measure the effect of background contrast modulation on the electrophysiological response of the retina to a dead leaves stimulus. ERG and VEP results were recorded using the FDA-approved Diagnosys clinical system (Diagnosys LLC, Lowell, MA, USA). The ERGs and VEPs were recorded without dilation, following the ISCEV recommendations for pattern ERGs/VEPs. The Dawson, Trick, and Litzkow (DTL) silver-nylon electrode was in contact with the bulbar conjunctiva and functioned as the active electrode in the experiment.

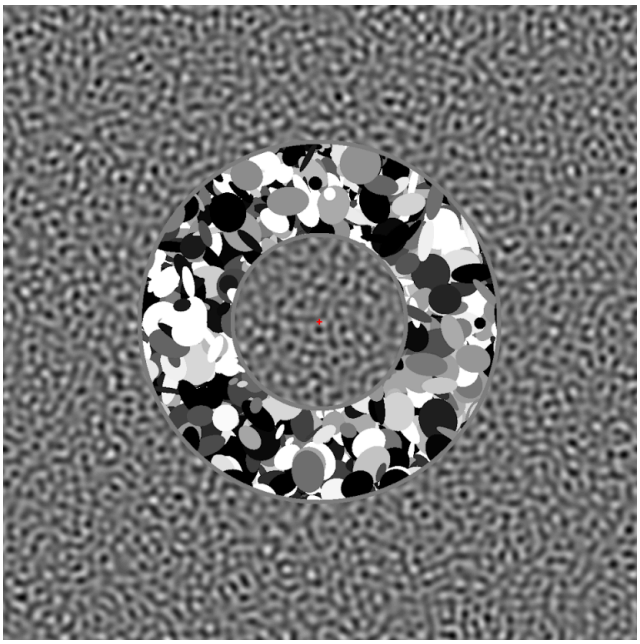

Figure 4.1. Representative stimulus for lateral ERG/VEP experiments tested at 6 deg eccentricity and 50% surround contrast. A continuous ring of dead leaves stimuli with a visual width of 4 deg when tested at 100 cm. The surrounding isotropic noise was presented at one of 4 contrast levels (here 50% contrast). A 0.25 deg buffer ring of isoluminant space was introduced between the stimulus and the surround to prevent edge effects.

Only the right eye of each subject was tested; the left eye was occluded with an eye patch. After cleaning and prepping the skin with alcohol wipes and exfoliation cream, two skin electrodes were used as a ground (3M Dot, forehead) and reference ERG electrodes (Diagnosys LLC, disposable skin electrode, ipsilateral temple). The ERG ground electrode was also used as a ground electrode for the VEPs. Two gold cup electrodes were used as the active and reference VEP electrodes, according to the 10/20 system.

The stimuli were presented on a 48" LG OLED monitor with a refresh rate of 120 Hz. A continuous ring of dead leaves stimuli (4 deg width) was presented at each of two mid-peripheral eccentricities: 6 or 10 deg at a viewing distance of 1 m. The dead leaves pattern contrast-reversed at a rate of 7.5 reversals/s (15 Hz) and an average contrast of 50% and it was surrounded with isotropic noise of varying contrast (0, 25, 50, and 75%) (Figure 4.1) that contrast-reversed at 1 reversal/s (2 Hz). Between the stimulus and the surround, a 0.25 deg ring of isoluminant, non-patterned space was inserted to prevent responses based on contrast reversal at the edge where the dead leaves and surrounding noise meet. ERGs were obtained with surround contrast of 0%, 25%, 50%, and 75%. The average luminance of the stimuli and background was held constant for all experimental conditions (75 cd/m^2). Fast Fourier transform was performed to isolate the 15 Hz harmonic corresponding to responses elicited by the dead leaves patterns. Surround contrast response curves were generated for each eccentricity. Area under the curve was calculated as trapezoids between each of the 4 contrast levels, resulting in three areas: 0025 (area from 0% to 25% surround contrast), 2550 (area from 25% to 50% surround contrast), and 5075 (area from 50% to 75% surround contrast) (Figure 4.2)

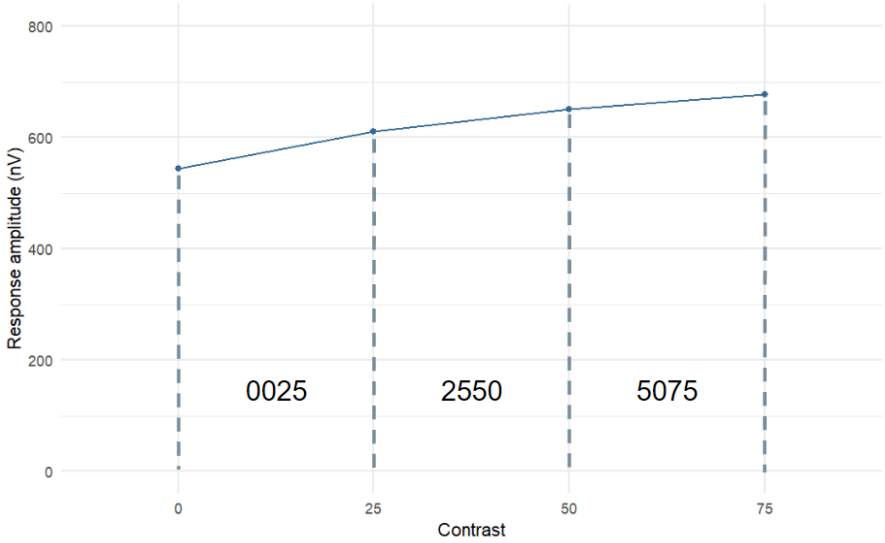

Figure 4.2. Example surround-contrast response function for electrophysiological experiments using sample ERG data from one subject at 6 deg eccentricity. Area under the curve was calculated as trapezoids between each of the 4 contrast levels, resulting in three areas: 0025 (area from 0% to 25% surround contrast), 2550 (area from 25% to 50% surround contrast), and 5075 (area from 50% to 75% surround contrast).

b. Oscillatory Potentials

To investigate the AC function, we recorded oscillatory potentials (OPs) from photopic full-field flash ERGs produced in a Ganzfeld stimulator. Single flash ON and OFF sawtooth stimuli were recorded over background luminance of 65 cd/m^2. based on established protocols for differentiating ON and OFF responses [68]. The peak luminance of each sawtooth stimulus presentation was 365 cd/m^2 with mean luminance of 215 cd/m^2. Stimuli were presented with 10 Hz frequency. For ON responses, peak luminance was reached at the beginning of each 100 ms interval with gradual decrease in luminance over 100 ms; rapid increase in luminance at the beginning of each interval elicited ON response (Figure 4.3). For OFF responses, peak luminance was reached at the end of each 100 ms interval with gradual increase in luminance over 100 ms; rapid decrease in luminance at the beginning of each interval elicited OFF

response. All responses were recorded using Espion analysis software. All ERGs were recorded with a wide bandwidth of temporal frequencies (1-1000 Hz). This allowed us to capture the high-frequency wavelets on the rising arm of the b-wave and isolate the OPs by applying a bandpass filter of 75-300 Hz [69]. Though not analyzed as part of this thesis, the variables of interest related to OPs were (1) amplitude and implicit time of each OP and (2) analysis of waveform via discrete wavelet transform (DWT) [70–72].

4.4 Electrophysiological Results

Retinal responses to a dead leaves contrast-reversing stimulus were recorded at 4 surround contrast levels (0%, 25%, 50%, and 75%) at the same 2 peripheral eccentricities (6 and 10 deg), totaling 8 stimuli. Electroretinography (ERG) and visual evoked potentials (VEP) were recorded simultaneously. From these, the area under the curve (AUC) was calculated as a sum of trapezoids for the following areas: (1) total of all surround contrast levels, (2) 0% to 25% contrast, (3) 25% to 50% contrast, and (4) 50% to 75% contrast. Each outcome was plotted against AXL and M (Figures 4.7 - 4.8, and Figures 4.10 - 4.11). Two-way ANOVA was calculated to assess group mean differences at three pedestal contrast levels (0 to 25%, 25 to 50%, and 50 to 75%) and two eccentricities (6 and 10 deg) for ERG (Figure 4.6) and VEP (Figure 4.9) results.

After selecting complete data sets and removing outliers, 19 subjects were included in the analysis of the ERG responses, and 16 subjects were included for VEP responses. Recall that an unconventional alpha cutoff of 0.40 was used, Spearman Rank correlations to identify the results that may merit follow-up research. For the electrophysiology experiment, the unconventional alpha was determined through power analysis utilizing the largest effect size of an outcome

correlation with AXL (primary outcome). Of outcomes related to electrophysiology, the greatest effect size was seen between AXL and the area under the VEP vs response curve at surround contrast level 5075 and 10 deg eccentricity (Rs = -0.418, Figure 4.10). Using this cutoff, we identify electrophysiological correlations that are interesting as it pertains to the role of lateral interactions in myopia.

No statistically significant differences were present between pedestal contrast levels or eccentric locations on ANOVA of ERG data (Figure 4.6, Table 4.1). For VEP data, a statistically significant overall difference in AUC was present between 6 and 10 deg eccentricity ($F = 14.48$, $p < 0.001$). Subsequent Tukey post-hoc analysis revealed a borderline significant difference between the lowest (0 to 25%) and highest (50 to 75%) contrast levels ($p = 0.049$). No statistically significant interaction effects were present between pedestal contrast levels or eccentric locations (Figure 4.9, Table 4.2).

No significant correlations were identified at any eccentricity or condition for ERGs (Figures 4.7 and 4.8). Based on our unconventional alpha cutoff of 0.4, a potentially interesting relationship was identified in the VEP data set between AXL and 5075 AUC (Figure 4.10). Another interesting relationship in the VEP data set was identified between M and 0025 AUC (Figure 4.11). Given the lack of a pattern between ERG and VEP results and a lack of coincidence in potentially interesting VEP results between AXL and M correlations, the effects noted here are less convincing.

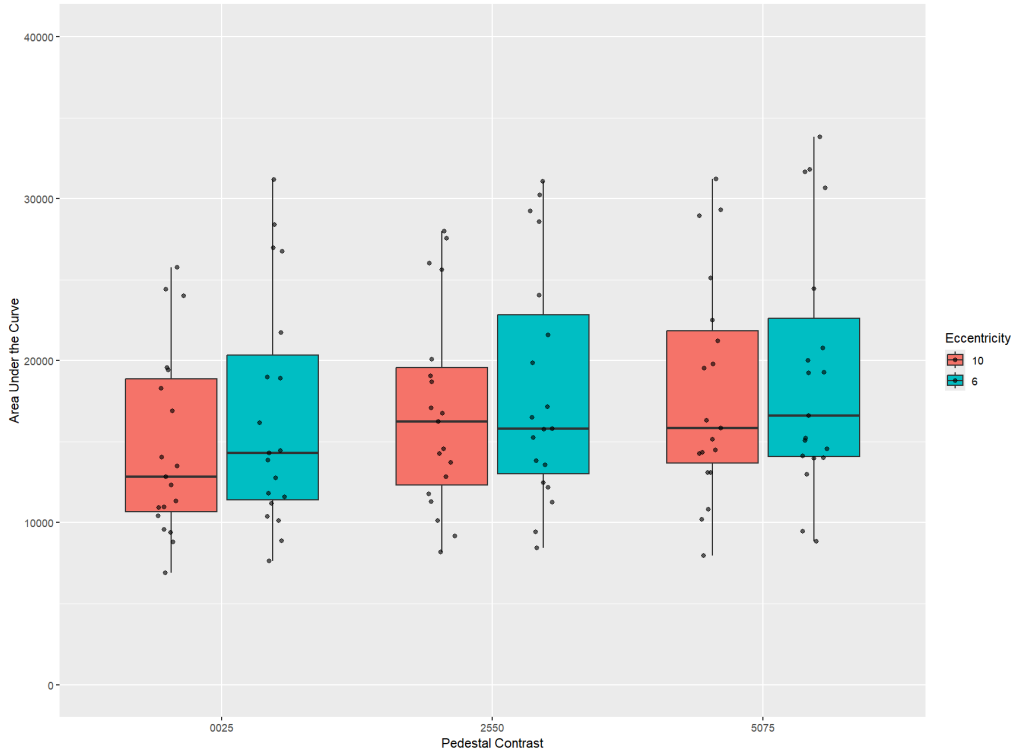

Figure 4.6. Comparison of area under the curve assessing ERG responses using two-way ANOVA. Assessed at three pedestal contrast levels (0 to 25%, 25 to 50%, and 50 to 75%) and two eccentricities (6 and 10 deg). No statistically significant differences were present between pedestal contrast levels or eccentric locations. Significance levels are as follows *** $p < 0.001$, ** $p < 0.01$, * $p < 0.05$. P-values are reported to three digits of precision.

Table 4.1. Summary statistics for ERG outcomes separated by eccentricity and surround contrast level. All parameters are reported with 3 digits of precision.

Variable	Eccentricity	Mean	SD	Min	Max
AUC.0025	6	16634.4	7184.98	7625.17	31186.4
AUC.0025	10	14706.0	5701.17	6917.82	25758.3
AUC.2550	6	18225.9	7238.16	8440.98	31079.6
AUC.2550	10	16896.3	6198.44	8189.29	27991.0
AUC.5075	6	19294.9	7713.57	8855.74	33816.4
AUC.5075	10	18060.9	6774.22	7971.53	31220.2
AUC.total	6	54155.2	21897.45	24921.89	93912.6
AUC.total	10	49663.3	18356.31	23078.63	83222.7

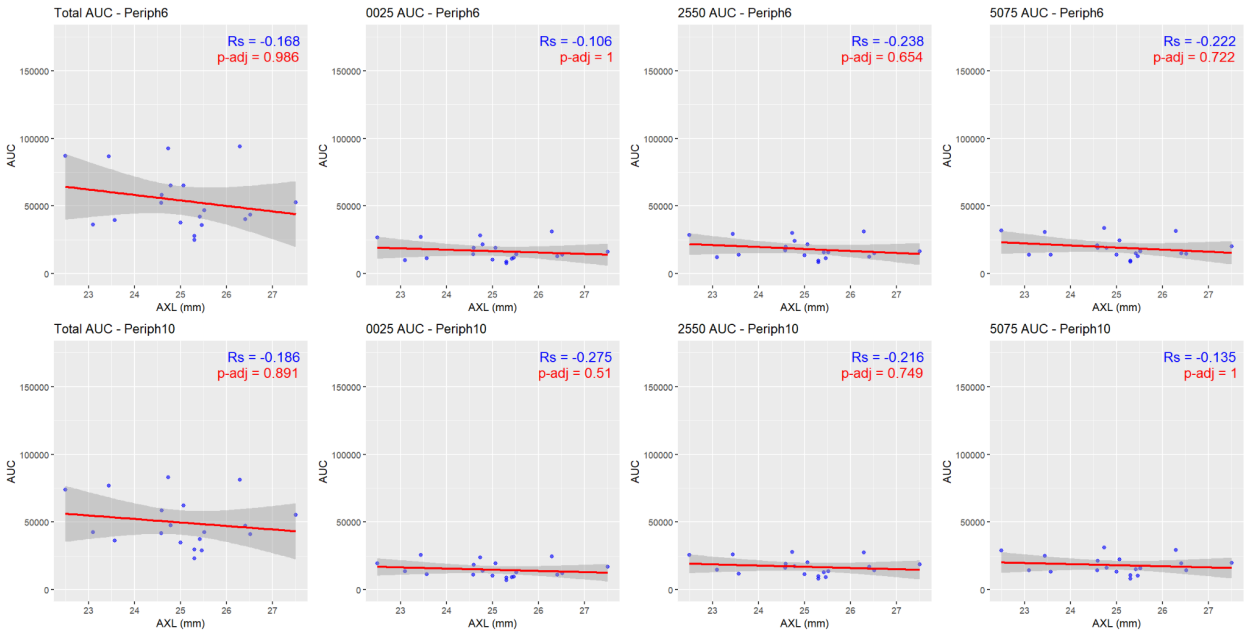

Figure 4.7. Spearman rank correlation of Lateral ERG (LERG) responses and axial length (AXL). No statistically significant relationships were found with AXL for any contrast level or eccentricity. P-values are adjusted for two eccentricities using Bonferroni method and reported to three digits of precision.

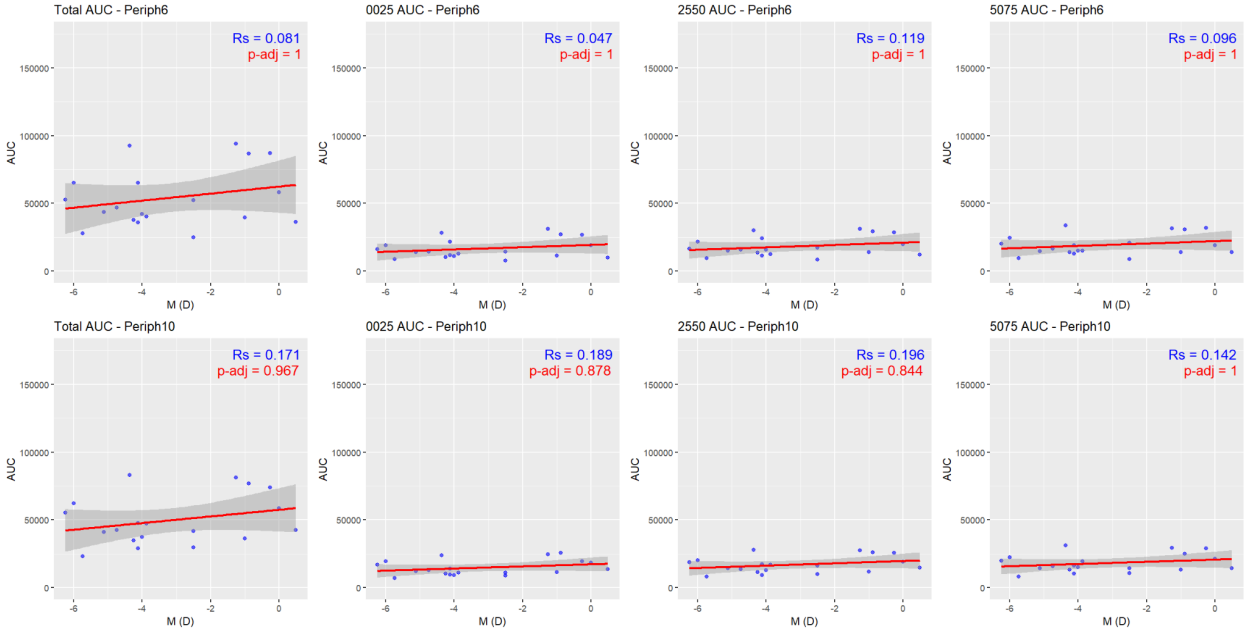

Figure 4.8. Spearman rank correlation of Lateral ERG (LERG) responses and spherical equivalent refractive error (M). No statistically significant relationships were found with M for any contrast level or eccentricity. P-values are adjusted for two eccentricities using Bonferroni method and reported to three digits of precision.

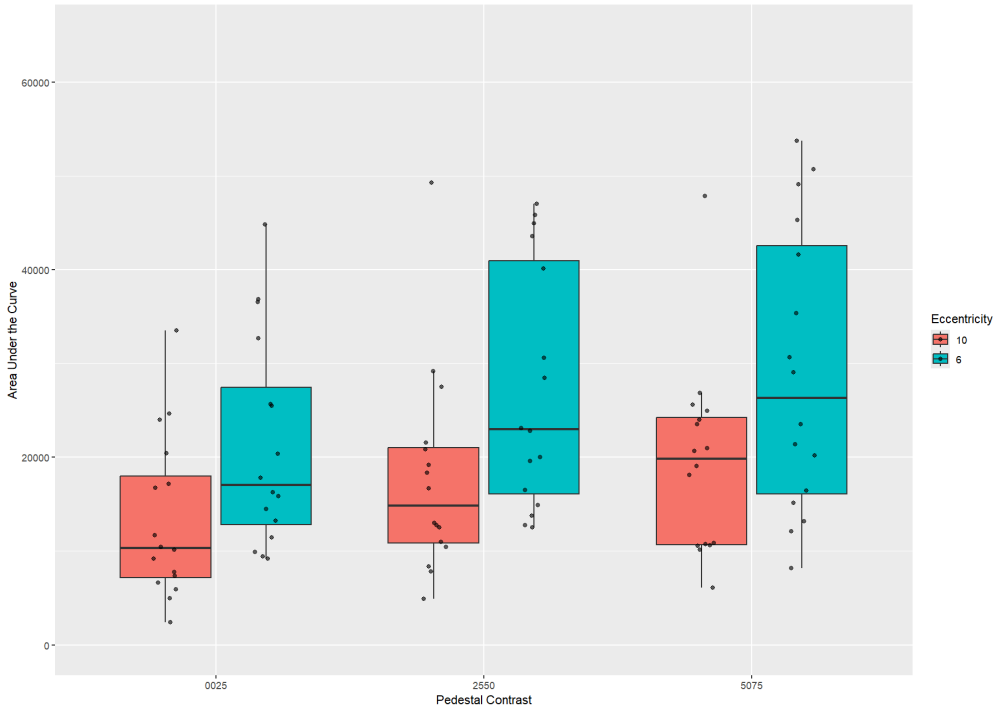

Figure 4.9. Comparison of area under the curve assessing VEP responses using two-way ANOVA. Assessed at three pedestal contrast levels (0 to 25%, 25 to 50%, and 50 to 75%) and two eccentricities (6 and 10 degrees). Overall a significant difference was found in the area under the curve between 6 and 10 degrees eccentricity ($p < 0.001$). There was a borderline significant difference between the lowest (0 to 25%) and highest (50 to 75%) contrast levels ($p = 0.049$). No statistically significant interaction effects were present between pedestal contrast levels or eccentric locations. Significance levels are as follows *** $p < 0.001$, ** $p < 0.01$, * $p < 0.05$. P-values are reported to three digits of precision.

Table 4.2. Summary statistics for VEP outcomes separated by eccentricity and surround contrast level. All parameters are reported with 3 digits of precision.

Variable	Eccentricity	Mean	SD	Min	Max
AUC.0025	6	21265.7	11210.42	9196.92	44830.5
AUC.0025	10	13315.1	8649.68	2407.20	33554.4
AUC.2550	6	27298.5	12960.30	12549.81	47034.1
AUC.2550	10	17718.7	10871.57	4896.14	49289.3
AUC.5075	6	29117.0	15145.97	8209.96	53756.4
AUC.5075	10	19420.5	10161.18	6101.69	47893.3
AUC.total	6	77681.2	38761.94	34850.77	138948.0
AUC.total	10	50454.3	28605.30	13405.02	130737.0

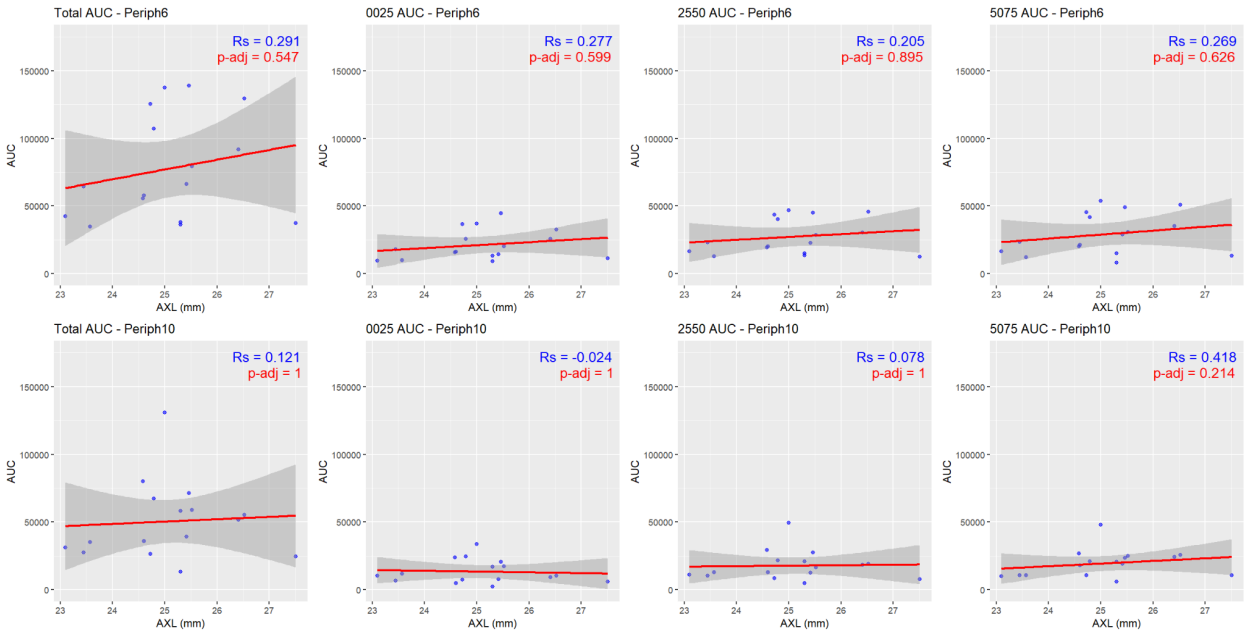

Figure 4.10. Spearman rank correlation of Lateral VEP (LVEP) responses axial length (AXL). No statistically significant relationships were found with AXL for any contrast level or eccentricity. P-values are adjusted for two eccentricities using Bonferroni method and reported to three digits of precision.

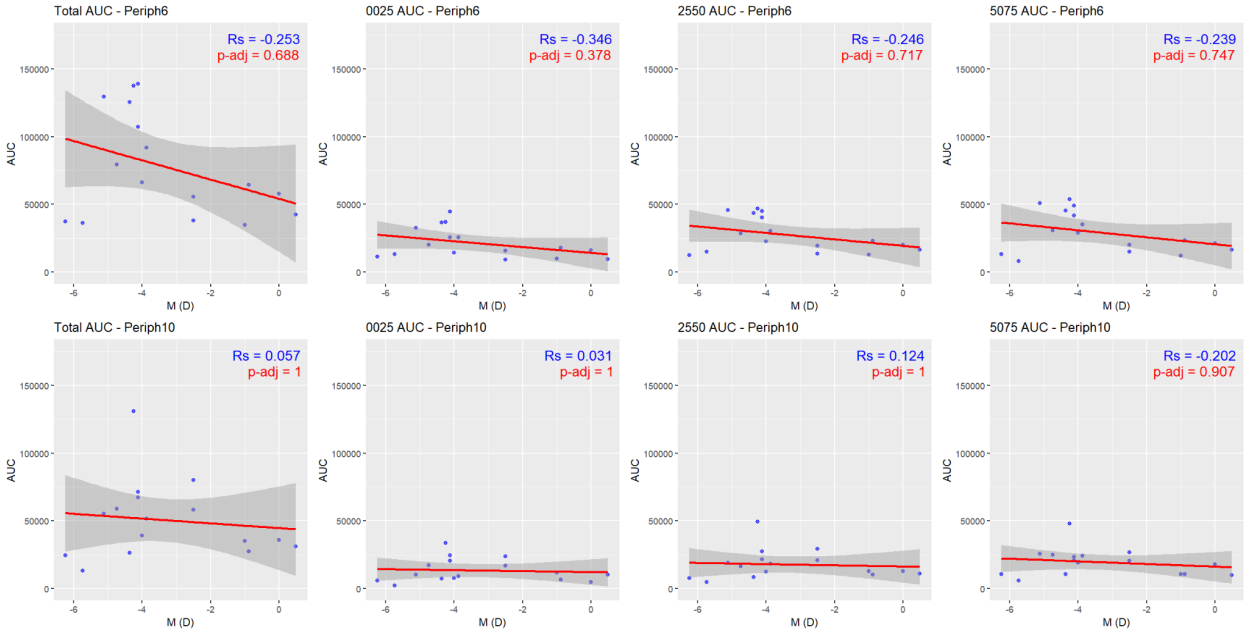

Figure 4.11. Spearman rank correlation of Lateral VEP (LVEP) responses spherical equivalent refractive error (M). No statistically significant relationships were found with M for any contrast level or combination of contrast levels. P-values are adjusted for two eccentricities using Bonferroni method and reported to three digits of precision.

5. Discussion

This study investigated the relationship of lateral interactions with ocular axial length in the human eye. To explore this relationship, novel methodologies were developed to investigate the effect of surround contrast on individual responses. One strength of this approach is that the overlap in stimulus design between psychophysical and electrophysiological experiments allows us to simultaneously investigate visual perception and objective responses. Additionally, the study explored these relationships in spatially discrete testing locations, informed by rising interest in mid-peripheral regions in the mechanism of human emmetropization.

A significant strength of the present study is the integration with a larger project investigating a comprehensive profile of retinal pathways. Pathways investigated by other researchers include investigations targeting (1) the magnocellular, parvocellular, and koniocellular ganglion cell pathways, (2) the ON and OFF pathways mediated in part by bipolar cells, and (3) adaptation effects of the outer-retina.

Due to the study's exploratory nature and logistical constraints, the study's sample size does not have sufficient statistical power to detect small effect sizes reliably. This is an important consideration for interpreting study results, as our study indicates that, while interesting, lateral interaction effects appear to be a small effect, if indeed they are present. This was addressed via the method outlined in section 3.6, specifically by identifying the largest effect size for a set of results. The use of this custom methodology developed during the study provides an important step forward, one that will open opportunities for further exploration of the effects outlined below. To strategically explore our results in light of sample size limitations, a power analysis was conducted to determine an unconventional p-value for each of the three testing categories.

Recall that this unconventional alpha cutoff for the CSF was $p < 0.10$, for the TvC was $p < 0.20$, and for ERG/VEP analysis was $p < 0.40$.

5.1 Experiment 1: Contrast Sensitivity Function

When measuring the monocular CSF, statistically significant results were found at 10 deg, but not at 6 deg eccentricity. For example, acuity, the high frequency cutoff of the CSF, demonstrated a significant negative correlation with AXL at 10 deg (Figure 4.7), where longer eyes had lower resolution at the high frequency cutoff. As expected, this coincides with a significant positive correlation of acuity with refractive error (M) at 10 deg (Figure 4.8). Also at 10 deg eccentricity, the AULCSF and AULCSF_LowPass (area under the low frequency cutoff) were significantly correlated with M. The trend toward greater significance at 10 deg versus 6 deg eccentricity suggests the possibility of a differential response between these mid-peripheral retinal loci.

Calculating the area under the CSF produced mixed, albeit interesting results, especially in the analysis of the low-frequency dropoff. As previously mentioned, positive correlations were present between M and both AULCSF and AULCSF_LowPass at 10 deg eccentricity. The corresponding relationship of AULCSF_LowPass and AXL exceeded a conventional alpha cutoff at 10 deg eccentricity (Figure 4.5), but was close enough to merit further investigation with a study with increased power. Correlations with AULCSF_LowPass are notable for at least three reasons: (1) the low frequency dropoff may be to the lateral interactions within the visual system, (2) relationships with total AULCSF are not as consistently present within the data set, and (3) no significant correlations were noted in the function's peak. If such an effect is present, the effect size is too small to detect given our sample size. A prospective power analysis was

conducted to determine what sample size would be necessary in subsequent studies to obtain a power of 0.80 at an alpha cutoff of 0.05. Based on the largest effect size seen in the present CSF data set for an outcome correlated with AXL, a minimum sample size of 34 subjects is necessary.

Therefore, two trends in the area under the CSF were noted. First, there is a trend toward stronger correlations at 10 deg than at 6 deg. This emphasizes the importance of testing responses at multiple mid peripheral locations to better understand the locations that may be important in emmetropization. A growing body of evidence suggests that there is a differential impact of foveal and peripheral retinal signalling on emmetropization [61,73,74]. The present study suggests that there may be even finer differences within classically mild peripheral eccentricities to explore. One limitation of the present study is that the sizes of the peripheral stimuli were not adjusted to account for cortical magnification. This was a strategic choice made so that the size of the psychophysical and electrophysiological stimuli were comparable and fitted in the screen. The screen size needed was already large given the peripheral eccentricities tested. Comparisons between eccentricities should therefore be taken with caution, as the sensitivities measured are not directly comparable. However, the trends noted here merit further exploration and future experiments should account for cortical magnification so that the results at the two separate eccentricities can be more readily compared [75–78].

Secondly, more consistent correlations are found between AXL and M with the AULCSF_LowPass than with the AULCSF. Though the two measures are inherently linked (AULCSF_LowPass being a subset of AULCSF), this trend highlights a need for further investigation into the characteristics of the low-frequency dropoff in emmetropization. Indeed, applying a low pass filter to the AULCSF is likely not the best method for assessing the

characteristics of the low-frequency dropoff, since the area under the curve is necessarily tied to the location of the peak.

At 10 deg eccentricity, a positive correlation of CSpeak and M was noted, where more myopic eyes showed a lower contrast sensitivity at the peak (CSpeak). This result is most notable as it relates to the AULCSF and AULCSF_LowPass results measured at 10 deg eccentricity because the AULCSF and AULCSF_LowPass measures are inherently related to the location of the peak. If the relationship between CSpeak and M is true, it may confound our assessment of the low-frequency cutoff. This does not negate the interesting correlations found between AULCSF_LowPass and AXL or M; however, it does reinforce the need for a more specific measure related to the rate of low-frequency dropoff to attempt to dissociate the two characteristics of the CSF curve.

The current analysis utilizes a symmetric curve fit, which may attenuate modulation of the low frequency dropoff to some extent. Future analysis of the low-frequency dropoff should consider applying an asymmetric curve fit to the CSF with targeted analysis of the low-frequency dropoff. From this, a parameter could be identified that approximates the dropoff rate as a metric for the effect of lateral interactions on attenuation of contrast sensitivity at low frequencies. This more complex analysis would differentiate between low-frequency characteristics from a subject's overall contrast sensitivity profile.

A preponderance of evidence suggests that processing of mid to low spatial frequencies (with most studies referring to spatial frequencies between 2 and 8 cpd) is implicated in retinal control of eye growth [59,74,79,80]. The present work reinforces the importance of analyzing the characteristics of the visual response at these spatial frequencies. Research into the retinal

emmetropization mechanisms also suggests that S cones may be involved [58,60,81], especially in extrafoveal and mid peripheral retinal locations [74,82]. Significantly, the spatial resolution of parafoveal S-cones is less than 5 cpd [59]. The present study did not specifically tailor the stimuli to active S cones, which can be accomplished using the silent-substitution method, but it does highlight the importance of the low frequencies in mid peripheral regions. This work suggests that very low spatial frequencies, even lower than 2 cpd, may merit further investigation as they may relate to longer axial lengths and more myopic refractive errors.

5.2 Experiment 2: Threshold versus Contrast (TvC) function

The experimental setup of the Threshold versus Contrast (TvC) function was specifically designed to assess the effect of surround contrast (pedestal contrast) on subjects' contrast thresholds. The effect of a surround on target detection is characterized as either "surround suppression" or "surround facilitation", with suppression being the most commonly recorded in the literature [83,84]. Previous work examining the differential effect of a surround between foveal and peripheral locations found that surround suppression increased with increasing eccentricity. The authors concluded that the difference in surround processing in the periphery versus the fovea may indicate distinct roles of these locations in visual processing [83]. The influence of surround processing on emmetropization has yet to be fully characterized, especially at mid peripheral locations. Given the known asymmetry of foveal and peripheral processing in emmetropization [60,61,73], such a dichotomy in the spatial distribution of center-surround processing raises the question of whether they might be implicated in the development of myopia.

The present study investigated the possible relationship between the processing of surround contrast and axial length. To that end, we measured contrast thresholds as a function of adjacent surround (pedestal) contrast level and assessed the effect through calculation of a dipper function (the TvC function). In an attempt to elucidate retinal versus cortical effects testing was conducted under monocular and dichoptic testing conditions, respectively.

At 6 deg eccentricity, weak associations were found between: (1) AXL and the area under the curve (AUTVC) tested dichoptically, as well as between (2) M and AUTVC monocularly; where more myopic/longer eyes were less sensitive to contrast overall in the presence of surround noise. This result would not be unexpected given our CSF results. However, in the absence of a pattern in monocular/dichoptic viewing conditions or between M and AXL, these correlations are less convincing.

The Intrinsic Noise (IN) of the visual system represents the baseline noise inherent in the contrast detection system that must be overcome in order for a subject to detect contrast. The origin may be optical, neural, or more likely a combination of both [85,86]. As previously described (see section 4.3), IN is the curve fit parameter of the TvC dipper function that accounts for the early decrease in contrast threshold toward the function's minimum. Therefore, a relationship between IN and AXL/M may indicate a difference in a visual system's ability to overcome internal variability, taking into account either the length of the eye or optical correction required.

It should be noted that intrinsic noise is typically measured by two methodologies: (1) as a function of a pedestal factor that is incorporated into the stimulus presentation structure (the TvC dipper function) [64], and (2) through masking of the stimulus using an overlying external noise component that spans the entire presentation screen [85,87]. In the present study, a TvC

function was used to assess the effect of the contrast of surrounding noise on an *adjacent* stimulus (Figure 3.4). That is to say that the stimulus whereby contrast thresholds were measured (in this case a sine-wave grating) did not overlap spatially with the surrounding isotropic noise. The logic in this design is that the information (contrast level) in the surround must be processed laterally in space in order to affect the contrast threshold to the gaussian sine-wave grating.

Therefore, the design inherent in this version of the TvC function is meant to approximate lateral interactions in visual processing. One limitation of our technique is the apparent summation effect that can be incurred through presentation of immediately adjacent stimuli [88]. Follow up studies might explore the introduction of a "buffer" ring between the grating target and surrounding isotropic noise, similar to the design of the electrophysiological stimulus in the present study (see section 4.1).

In the present study, a dichotomy was found in the relationship between IN and AXL where positive correlations were found at both 6 and 10 degrees eccentricity, but only under dichoptic conditions. Therefore, when inter-eye processing is involved, longer eyes tended to have higher IN than shorter eyes. No such relationship was noted between IN and AXL under monocular testing conditions. Unsurprisingly, IN was also negatively correlated with M; though these were found under both monocular and dichoptic conditions, where more myopic eyes tended to have higher intrinsic noise at both mid-peripheral eccentricities. These data are suggestive of a relationship between Intrinsic Noise in the visual system and myopia in the mid peripheral retina as measured through the TvC pedestal method. Given the known differential between foveal and mid peripheral center-surround processing [83], our data begs the question, "Does a similar association between IN and AXL exist at the fovea?" Analysis of the foveal data

set including differences between the foveal and mid peripheral data set is certainly worth exploring.

Another question worth exploring is the relative contribution of optical and neural components to the Intrinsic Noise in this experiment. It could be that the noise occurs within the visual system; if that were the case, a true dichotomy between monocular and dichoptic conditions may indicate that this noise originates at downstream processing centers, such as the visual cortex. Alternatively, the optics of the system may contribute. Single vision spectacles are known to cause greater peripheral retinal defocus with longer axial lengths, though if the spectacles produced the effect, one would expect to see a monocular relationship as well. One optical component that may influence inter-ocular processing, but not monocular processing might be our use of polarizers. It could be that small vergence eye movement errors (phoria) could alter the retinal loci of stimuli so that they do not perfectly align peripherally between the two eyes, causing an increase in variability in cortical but not retinal responses. Future work may consider using an alternative system for controlling monocular/dichoptic presentation, such as shutter glasses) to see if the monocular/dichoptic dichotomy persists. It may also be that the resolution of the study was simply not enough to identify true correlations with AXL under monocular conditions. Though the origin of the current results are unknown, the role of intrinsic noise and perhaps also perceptual adaptation to this noise are worth exploring further.

The sensitivity of the visual system to changes in contrast (Psi) is represented by the rising arm of the TvC dipper function following the minimum and is guided by Weber's Law. A higher Psi can be thought of as lower impact of differences in surround contrast, and vice versa. A weak positive correlation was noted between Psi and AXL at 6 deg eccentricity when noted dichoptically. Should this association prove consistent in follow up studies, this would indicate

that longer eyes are more sensitive to changes in surround contrast. However, this effect does not occur at 10 deg dichoptically or at either eccentricity under monocular viewing conditions. Likewise, no relationships are identified between Psi and M at any eccentricity or viewing condition. One limitation of this analysis is a floor effect that was noted in the Psi data set, which may attenuate a true correlation between the two variables. This effect may be due to insufficient sampling above the pedestal contrast at the minimum. In the current protocol, we find that the surround (pedestal) contrast at the minimum falls around 0.3 under both monocular (Mean 6 deg 0.240 +/- 0.099, 10 deg 0.301 +/- 0.137) and dichoptic conditions (Mean 6 deg 0.291 +/- 0.132, 10 deg 0.269 +/- 0.110). Since Psi is associated with the rising arm of the dipper function, it is possible that increased sampling above 0.32 is necessary, as we currently test only one additional surround contrast level (0.68 contrast). Future work should attempt to optimize parameters to ensure a more accurate estimate of Psi.

The location of the TvC minimum is characterized by the surround (pedestal) contrast (minPedes) and the contrast threshold (MinThresh). A weak association was found between minPedes and M when tested at 10 deg eccentricity under dichoptic condition, where longer eyes reached a minimum contrast threshold at a lower pedestal contrast than shorter eyes. If such an association did exist, it would indicate that longer eyes are better tuned to stimulus detection in conditions where the surrounding environment has lower contrast. However, in the absence of a coincident association under any other testing condition or with AXL findings, this finding is less convincing.

Another dichotomy in the monocular versus dichoptic stimuli was noted in the contrast threshold at the function minimum (MinThresh). Promising associations were noted between MinThresh and AXL at both 6 and 10 degrees, but only when tested under dichoptic conditions.

Here, longer eyes showed higher contrast thresholds at the function minimum. In other words, the maximum contrast sensitivity reached may be lower in myopes versus emmetropes. As previously discussed, the origin of a differential effect under dichoptic and monocular testing is not known, since they could be due to a true neural effect, optical considerations, insufficient resolution of statistical testing, or another unknown factor. Of note, associations between MinThresh and and M were noted under both monocular and dichoptic conditions, but only at 6 deg eccentricity. It would not be unexpected for the contrast threshold at the minimum (MinThresh) to be related to AXL and M, however the apparent dichotomy between dichoptic and monocular results merits further inquiry [65].

A limitation of the TvC stimulus design was our choice of spatial frequency. Based on an initial review of the literature [89,90], we anticipated a peak spatial frequency in the midperiphery close to 4 cpd. However, our results from experiment 1 (CSF) indicate that the true peak spatial frequency for this grating design was 1.212 ± 0.278 cpd at 6 deg and 1.075 ± 0.286 cpd at 10 deg (Table 2.1). A more ideal spatial frequency for the Gaussian grating may be 1 cpd. However, if we were to set the spatial frequency of the TvC stimulus at 1 cpd, the number of cycles in the stimulus would likely be too low to accurately determine contrast threshold [58,91]. Future experiments should explore how the stimulus diameter (in this case 4 deg) might be altered to accommodate a more appropriate spatial frequency for mid peripheral testing.

5.3 Experiment 3: Electrophysiology

Though select VEP findings were found to have interesting correlations with AXL and/or M, using our unconventional alpha cutoff of 0.4, there was no logical pattern present. Therefore,

the relationships between AXL and M and electrophysiology results are less convincing than the psychophysical results.

The development of novel methodology to assess lateral interactions was both a strength and a limitation of the present study. The development of such methods is a much-needed advancement in electrophysiological study and makes a key contribution to the field of using electrophysiology to assess the emmetropization process.

Our design explores lateral interactions and provides a method for spatially discrete testing. The limitations of this approach are two-fold. First, the probable effect size is likely too small to be detected by our sample size (n = 19). Though spatially discrete testing is certainly a strength of the present methods, the process of isolating a distinct ring within visual space decreases the magnitude of possible retinal summation compared to full-field techniques.

Our analysis based on the largest ERG/VEP effect size to select an unconventional alpha suggests that in follow-up studies, a sample of at least 42 subjects is required to obtain a power of 80% and an alpha cutoff of 0.05. The present results may indicate that there is no relationship between emmetropization and the Lateral ERG/VEP responses or that the sample was too small to detect such an effect.

Secondly, unlike other ERG methods, we do not have the option to rely on previous validation studies. Our sample size was limited by the need for methodological refinement about halfway through the data collection. Specifically, the isoluminant buffer space was introduced at this juncture. The methods presented here are the final version of the process we developed during the course of the study. Further studies are necessary to properly characterize the stimulus and determine ideal testing conditions. One characteristic we are particularly interested in is the

effect of the sizing of the isoluminant buffer ring. For the present study, a small ring size was chosen with the explicit intention of disrupting contrast-reversal edge effects. A follow-up study is planned to determine at what size the buffer ring interrupts lateral processing and extinguishes the effect of surround contrast on the stimulus response. Though no statistically significant correlations were found between AXL or M and ERG or VEP responses in the present study, this work is worth revisiting with a larger sample size.

6. Conclusions

Overall, we find that the psychophysical measures of lateral interactions explored in this experiment may be related to axial length and refractive error. The contrast sensitivity at low spatial frequencies is especially promising, perhaps indicating that the lateral interactions contributing to the low spatial frequency dropoff of the CSF may be increased with increasing axial length. Though we find that some psychophysical measures related to the effect of surround contrast on grating perception are promising, this relationship is not seen in the electrophysiological studies. Further work is needed to solidify our understanding of these interactions and where relationships with axial length may originate in the visual pathway.

7. References

1. Fredrick, D. R. Myopia. *BMJ* **324**, 1195–1199 (2002).
2. Li, Q. *et al.* Form-deprivation myopia downregulates calcium levels in retinal horizontal cells in mice. *Exp. Eye Res.* **218**, 109018 (2022).
3. Cho, B.-J., Shin, J. Y. & Yu, H. G. Complications of Pathologic Myopia. *Eye Contact Lens* **42**, 9 (2016).
4. Chamberlain, P., Lazon de la Jara, P., Arumugam, B. & Bullimore, M. A. Axial length targets for myopia control. *Ophthalmic Physiol. Opt.* **41**, 523–531 (2021).
5. Grosvenor, T. & Goss, D. A. Role of the Cornea in Emmetropia and Myopia. *Optom. Vis. Sci.* **75**, 132 (1998).
6. Grosvenor, T. & Scott, R. Role of the axial length/corneal radius ratio in determining the refractive state of the eye. *Optom. Vis. Sci.* **71**, 573–579 (1994).
7. Baird, P. N., Schäche, M. & Dirani, M. The GEnes in Myopia (GEM) study in understanding the aetiology of refractive errors. *Prog. Retin. Eye Res.* **29**, 520–542 (2010).
8. Cao, K., Wan, Y., Yusufu, M. & Wang, N. Significance of Outdoor Time for Myopia Prevention: A Systematic Review and Meta-Analysis Based on Randomized Controlled Trials. *Ophthalmic Res.* **63**, 97–105 (2020).
9. Jonas, J. B. *et al.* IMI Prevention of Myopia and Its Progression. *Invest. Ophthalmol. Vis. Sci.* **62**, 6 (2021).
10. Jones, L. A. *et al.* Parental History of Myopia, Sports and Outdoor Activities, and Future Myopia. *Invest. Ophthalmol. Vis. Sci.* **48**, 3524–3532 (2007).
11. Logan, N. S. *et al.* IMI Accommodation and Binocular Vision in Myopia Development and Progression. *Invest. Ophthalmol. Vis. Sci.* **62**, 4 (2021).

12. Rose, K. A. *et al.* Myopia, Lifestyle, and Schooling in Students of Chinese Ethnicity in Singapore and Sydney. *Arch. Ophthalmol.* **126**, 527–530 (2008).
13. Wallman, J., Gottlieb, M. D., Rajaram, V. & Fugate-Wentzek, L. A. Local Retinal Regions Control Local Eye Growth and Myopia. *Science* **237**, 73–77 (1987).
14. Aleman, A. C., Wang, M. & Schaeffel, F. Reading and Myopia: Contrast Polarity Matters. *Sci. Rep.* **8**, 10840 (2018).
15. Troilo, D., Gottlieb, M. D. & Wallman, J. Visual deprivation causes myopia in chicks with optic nerve section. *Curr. Eye Res.* **6**, 993–999 (1987).
16. Wildsoet, C. F. & Pettigrew, J. Experimental myopia and anomalous eye growth patterns unaffected by optic nerve section in chickens. *Clin. Vis. Sci.* **3**, 99–107 (1988).
17. Davies, N. P. & Morland, A. B. The Hermann-Hering grid illusion demonstrates disruption of lateral inhibition processing in diabetes mellitus. *Br. J. Ophthalmol.* **86**, 203–208 (2002).
18. Foley, J. M. Lateral effects in pattern vision. *J. Vis.* **19**, 8 (2019).
19. Heckenlively, J. R. & Arden, G. B. *Principles and Practice of Clinical Electrophysiology of Vision, Second Edition*. (MIT Press, 2006).
20. Hubel, D. H. & Wiesel, T. N. Receptive fields of optic nerve fibres in the spider monkey. *J. Physiol.* **154**, 572–580 (1960).
21. Jacobs, A. L. & Werblin, F. S. Spatiotemporal Patterns at the Retinal Output. *J. Neurophysiol.* **80**, 447–451 (1998).
22. Roska, B., Nemeth, E., Orzo, L. & Werblin, F. S. Three Levels of Lateral Inhibition: A Space–Time Study of the Retina of the Tiger Salamander. *J. Neurosci.* **20**, 1941–1951 (2000).
23. Strausfeld, N. J. & Campos-Ortega, J. A. Vision in Insects: Pathways Possibly Underlying

Neural Adaptation and Lateral Inhibition. *Science* **195**, 894–897 (1977).

24. Wagner, H.-J. The connectivity of cones and cone horizontal cells in a mosaic-type teleost retina. *Cell Tissue Res.* **175**, 85–100 (1976).
25. Werblin, F. S. & Dowling, J. E. Organization of the retina of the mudpuppy, Necturus maculosus. II. Intracellular recording. *J. Neurophysiol.* **32**, 339–355 (1969).
26. DeValois, R. L. & DeValois, K. K. *Spatial Vision*. (OUP USA, 1990).
27. Lin, Y.-S., Chen, C.-C. & Greenlee, M. W. The role of lateral modulation in orientation-specific adaptation effect. *J. Vis.* **22**, 13 (2022).
28. Baldwin, A. S., Meese, T. S. & Baker, D. H. The attenuation surface for contrast sensitivity has the form of a witch's hat within the central visual field. *J. Vis.* **12**, 23 (2012).
29. Boynton, G. M., Demb, J. B., Glover, G. H. & Heeger, D. J. Neuronal basis of contrast discrimination. *Vision Res.* **39**, 257–269 (1999).
30. Calcagni, A. *et al.* Colour contrast sensitivity in eyes at high risk of neovascular age-related macular degeneration. *Eur. J. Ophthalmol.* **30**, 1487–1494 (2020).
31. Chen, Q., Pei, Z., Koren, D. & Wei, W. Stimulus-dependent recruitment of lateral inhibition underlies retinal direction selectivity. *eLife* **5**, e21053 (2016).
32. Edwin Dickinson, J., Martin, R. A. & Badcock, D. R. Lateral inhibition between banks of orientation selective channels predicts shape context effects: A tilt-illusion field. *Vision Res.* **192**, 107975 (2022).
33. Montolio, F. G. J., Meems, W., Janssens, M. S. A., Stam, L. & Jansonius, N. M. Lateral Inhibition in the Human Visual System in Patients with Glaucoma and Healthy Subjects: A Case-Control Study. *PLOS ONE* **11**, e0151006 (2016).
34. Feldkaemper, M. & Schaeffel, F. An updated view on the role of dopamine in myopia. *Exp.*

Eye Res. **114**, 106–19 (2013).

35. Barathi, V. A. *et al.* Involvement of GABA Transporters in Atropine-Treated Myopic Retina As Revealed by iTRAQ Quantitative Proteomics. *J. Proteome Res.* **13**, 4647–4658 (2014).
36. Zhi, Z. *et al.* The Role of Retinal Connexins Cx36 and Horizontal Cell Coupling in Emmetropization in Guinea Pigs. *Invest. Ophthalmol. Vis. Sci.* **62**, 27 (2021).
37. Li, Y. *et al.* RNA-sequencing analysis reveals the long noncoding RNA profile in the mouse myopic retina. *Front. Genet.* **13**, 1014031 (2022).
38. Ashby, R. S. & Feldkaemper, M. P. Gene Expression within the Amacrine Cell Layer of Chicks after Myopic and Hyperopic Defocus. *Invest. Ophthalmol. Vis. Sci.* **51**, 3726–3735 (2010).
39. Chakraborty, R. *et al.* Melanopsin modulates refractive development and myopia. *Exp. Eye Res.* **214**, 108866 (2022).
40. Chen, J. C., Brown, B. & Schmid, K. L. Evaluation of inner retinal function in myopia using oscillatory potentials of the multifocal electroretinogram. *Vision Res.* **46**, 4096–4103 (2006).
41. Feldkaemper, M. & Schaeffel, F. An updated view on the role of dopamine in myopia. *Exp. Eye Res.* **114**, 106–119 (2013).
42. Huang, F. *et al.* Retinal Dopamine D2 Receptors Participate in the Development of Myopia in Mice. *Invest. Ophthalmol. Vis. Sci.* **63**, 24 (2022).
43. Lan, W., Yang, Z., Feldkaemper, M. & Schaeffel, F. Changes in dopamine and ZENK during suppression of myopia in chicks by intense illuminance. *Exp. Eye Res.* **145**, 118–124 (2016).
44. Liu, H., Schaeffel, F., Yang, Z. & Feldkaemper, M. P. GABAB Receptor Activation Affects Eye Growth in Chickens with Visually Induced Refractive Errors. *Biomolecules* **13**, 434 (2023).

45. Tkatchenko, A. V. *et al.* APLP2 Regulates Refractive Error and Myopia Development in Mice and Humans. *PLOS Genet.* **11**, e1005432 (2015).

46. Yang, J. *et al.* Advances in biomedical study of the myopia-related signaling pathways and mechanisms. *Biomed. Pharmacother. Biomedecine Pharmacother.* **145**, 112472 (2022).

47. Usmani, H., Patterson, S. S., Giamarco, M. M., Neitz, J. & Kuchenbecker, J. A. Electrophysiological evidence for GABA mediated feed forward transmission as a major cone signal ON pathway in the outer retina. (2022).

48. Duan, M.-M., Liu, H. & Zhong, Y.-L. Effect of shape deprivation on retinal thickness in myopic mice using an OCT method. *Front. Neurosci.* **17**, 1156990 (2023).

49. Kirik, F., Ekinci, C., Akbulut, E., Bayraktar, H. & Ozdemir, H. Regional analysis of segmented-macular structure in patients with myopic anisometropia. *Int. Ophthalmol.* **41**, 3713–3726 (2021).

50. Szigeti, A. *et al.* The Effect of Axial Length on the Thickness of Intraretinal Layers of the Macula. *PLOS ONE* **10**, e0142383 (2015).

51. Chan, K. *et al.* Vigabatrin-Induced Retinal Functional Alterations and Second-Order Neuron Plasticity in C57BL/6J Mice. *Invest. Ophthalmol. Vis. Sci.* **61**, 17 (2020).

52. Deniz, S. *et al.* Mammalian retinal horizontal cells are unconventional GABAergic neurons. *J. Neurochem.* **116**, 350–62 (2011).

53. Cheng, N., Tsunenari, T. & Yau, K.-W. Intrinsic light response of retinal horizontal cells of teleosts. *Nature* **460**, 899–903 (2009).

54. Chapot, C. A., Euler, T. & Schubert, T. How do horizontal cells ‘talk’ to cone photoreceptors? Different levels of complexity at the cone–horizontal cell synapse. *J. Physiol.* **595**, 5495–5506 (2017).

55. Thibos, L. N., Wheeler, W. & Horner, D. Power vectors: An application of fourier analysis to the description and statistical analysis of refractive error. *Optom. Vis. Sci.* **74**, 367–375 (1997).
56. Murrell, P. *R Graphics*. (Chapman & Hall/CRC, Boca Raton, Fla., 2006).
57. Cleveland, W. S. Graphical Methods for Data Presentation: Full Scale Breaks, Dot Charts, and Multibased Logging. *Am. Stat.* **38**, 270–280 (1984).
58. Taylor, C. P., Shepard, T. G., Rucker, F. J. & Eskew, R. T. Sensitivity to S-Cone Stimuli and the Development of Myopia. *Investig. Opthalmology Vis. Sci.* **59**, 4622 (2018).
59. Humanski, R. A. & Wilson, H. R. Spatial frequency mechanisms with short-wavelength-sensitive cone inputs. *Vision Res.* **32**, 549–560 (1992).
60. Schaeffel, F. & Swiatczak, B. Mechanisms of emmetropization and what might go wrong in myopia. *Vision Res.* **220**, 108402 (2024).
61. Panorgias, A. *et al.* Retinal Responses to Simulated Optical Blur Using a Novel Dead Leaves ERG Stimulus. doi:10.1167/iovs.62.10.1.
62. Ichhpujani, P., Parmar, U. P. S., Singh, R. B. & Kumar, S. Assessment of central and peripheral contrast sensitivity in myopes using Spaeth/Richman contrast sensitivity. *Oman J. Ophthalmol.* **18**, 16–21 (2025).
63. Kerber, K. L., Thorn, F., Bex, P. J. & Vera-Diaz, F. A. Peripheral contrast sensitivity and attention in myopia. *Vision Res.* **125**, 49–54 (2016).
64. Maiello, G., Walker, L., Bex, P. J. & Vera-Diaz, F. A. Blur perception throughout the visual field in myopia and emmetropia. *J. Vis.* **17**, 1–13 (2017).
65. Zhou, W.-D. *et al.* Cone mosaic in eyes with varied axial length using adaptive optics scanning laser ophthalmoscopy. *Photodiagnosis Photodyn. Ther.* **52**, 104517 (2025).

66. Azzopardi, P. & Cowey, A. Preferential representation of the fovea in the primary visual cortex. *Nature* **361**, 719–721 (1993).

67. Yan, F.-F. *et al.* Perceptual learning improves neural processing in myopic vision. *J. Vis.* **15**, 12 (2015).

68. Sustar, M. *et al.* ISCEV extended protocol for the photopic On–Off ERG. *Doc. Ophthalmol.* **136**, 199–206 (2018).

69. Gauthier, M., Gauvin, M., Lina, J.-M. & Lachapelle, P. The effects of bandpass filtering on the oscillatory potentials of the electroretinogram. *Doc. Ophthalmol. Adv. Ophthalmol.* **138**, 247–254 (2019).

70. Gauvin, M., Little, J. M., Lina, J.-M. & Lachapelle, P. Functional decomposition of the human ERG based on the discrete wavelet transform. *J. Vis.* **15**, 14 (2015).

71. Gauvin, M., Lina, J.-M. & Lachapelle, P. Advance in ERG analysis: from peak time and amplitude to frequency, power, and energy. *BioMed Res. Int.* **2014**, 246096 (2014).

72. Gauvin, M. *et al.* Assessing the Contribution of the Oscillatory Potentials to the Genesis of the Photopic ERG with the Discrete Wavelet Transform. *BioMed Res. Int.* **2016**, 2790194 (2016).

73. Smith, E. L. *et al.* Effects of Foveal Ablation on Emmetropization and Form-Deprivation Myopia. *Investig. Opthalmology Vis. Sci.* **48**, 3914 (2007).

74. Chen, Y., Lan, W. & Schaeffel, F. Size of the foveal blue scotoma related to the shape of the foveal pit but not to macular pigment. *Vision Res.* **106**, 81–89 (2015).

75. Jigo, M., Tavdy, D., Himmelberg, M. M. & Carrasco, M. Cortical magnification eliminates differences in contrast sensitivity across but not around the visual field. *eLife* **12**, e84205 (2023).

76. Virsu, V., Näsänen, R. & Osmoviita, K. Cortical magnification and peripheral vision. *J. Opt. Soc. Am. A* **4**, 1568 (1987).

77. Pointer, J. S. THE CORTICAL MAGNIFICATION FACTOR AND PHOTOPIC VISION. *Biol. Rev.* **61**, 97–119 (1986).

78. Pointer, J. S. & Hess, R. F. The contrast sensitivity gradient across the human visual field: With emphasis on the low spatial frequency range. *Vision Res.* **29**, 1133–1151 (1989).

79. Swiatczak, B. & Schaeffel, F. Emmetropic, But Not Myopic Human Eyes Distinguish Positive Defocus From Calculated Blur. *Investig. Opthalmology Vis. Sci.* **62**, 14 (2021).

80. Kwon, M. & Legge, G. E. Spatial-frequency requirements for reading revisited. *Vision Res.* **62**, 139–147 (2012).

81. Swiatczak, B. & Schaeffel, F. Myopia: why the retina stops inhibiting eye growth. *Sci. Rep.* **12**, 21704 (2022).

82. Graef, K. & Schaeffel, F. Control of accommodation by longitudinal chromatic aberration and blue cones. *J. Vis.* **12**, 14–14 (2012).

83. Xing, J. & Heeger, D. J. Center-surround interactions in foveal and peripheral vision. *Vision Res.* **40**, 3065–3072 (2000).

84. Cannon, M. W. & Fullenkamp, S. C. Spatial interactions in apparent contrast: Individual differences in enhancement and suppression effects. *Vision Res.* **33**, 1685–1695 (1993).

85. Pelli, D. G. & Farell, B. Why use noise? *J. Opt. Soc. Am. A* **16**, 647 (1999).

86. Radhakrishnan, H. & Pardhan, S. Contrast detection in noise with positive and negative defocus in myopes. *Vision Res.* **46**, 2949–2955 (2006).

87. Bennett, P. J., Sekuler, A. B. & Ozin, L. Effects of aging on calculation efficiency and equivalent noise. *J. Opt. Soc. Am. A* **16**, 654 (1999).

88. Taylor, C. P., Bennett, P. J. & Sekuler, A. B. Evidence for adjustable bandwidth orientation channels. *Front. Psychol.* **5**, (2014).

89. Rovamo, J. Cortical magnification factor and contrast sensitivity to luminance-modulated chromatic gratings. *Acta Physiol. Scand.* **119**, 365–71 (1983).

90. Virsu, V., Rovamo, J., Laurinen, P. & Näsänen, R. Temporal contrast sensitivity and cortical magnification. *Vision Res.* **22**, 1211–7 (1982).

91. Watson, A. B. Visual detection of spatial contrast patterns: Evaluation of five simple models. *Opt. Express* **6**, 12 (2000).

Appendix 1: ARVO 2024 abstract and poster on electrophysiology design

“Purpose: Despite the critical role of lateral interactions in retinal processing, there is no validated electroretinogram (ERG) to specifically probe this function. Using a novel ERG paradigm, we investigated the effect of background contrast on center-surround retinal response mechanisms elicited by a series of pattern-reversing stimuli.

Methods: Seven subjects (age 27 +/- 2, range 25-32 years) underwent a thorough vision screening. All subjects had BCVA 20/20 or better and no ocular pathology or vision deficit other than refractive error. The ERG stimuli were presented on a 48” LG OLED monitor with a 120 Hz refresh rate. A ring of 8 circular dead leaves stimuli (4 deg diameter each) was presented at each of two mid-peripheral eccentricities: 6 or 10 deg. The dead leaves pattern contrast reversed at a rate of 7.5 reversals/s (15 Hz) and an average contrast of 50%. The background pattern of isotropic noise (see figure) contrast-reversed at 1 reversal/s (2 Hz). ERGs were obtained with background contrast of 0%, 25%, 50%, and 75%. The average luminance of the stimuli and background were held constant for all experimental conditions (75 cd/m2). ERGs were recorded monocularly with a DTL electrode and an undilated pupil. Skin electrodes were used for ground and reference. Fast Fourier transform was performed to isolate the 15 Hz harmonic corresponding to retinal responses elicited by the dead leaves patterns. Background contrast response curves were generated for each eccentricity.

Results: At 6-deg eccentricity, the amplitude of the 15 Hz harmonic increases in a monotonic/linear relationship with background contrast ($R^2 = 0.8825$). ERG responses doubled from baseline (0%) to 75% background contrast condition (ratio: 2). The results from the 10-deg condition showed a biphasic change as a function of background contrast. Although retinal responses increased from baseline to 75% background contrast (ratio of 1.3) responses decreased from baseline to 25% (ratio: 0.5) and 50% (ratio: 0.88) background contrast, indicating an inhibitory relationship.

Conclusions: These findings suggest center-surround interactions in retinal processing independent of changes in mean luminance as well as a possible method for evaluating lateral interactions using ERG. Such methodology would be useful for analysis of functional deficits in the retina that may not be readily apparent on a structural level.

This abstract was presented at the 2024 ARVO Annual Meeting, held in Seattle, WA, May 5-9, 2024."

Reference:
Rachel Harmon, Fuensanta A Vera-Diaz, Thanasis Panorgias; Lateral interactions in the human retina assessed using a novel ERG paradigm. Invest. Ophthalmol. Vis. Sci. 2024;65(7):5852.

Figure 1. ARVO 2024 Poster

NECO | New England College of Optometry

Lateral Interactions in the Human Retina Assessed Using a Novel ERG Paradigm

5852

Rachel Harmon[1], Fuensanta A. Vera-Diaz[1], Thanasis Panorgias[1]
[1]New England College of Optometry, Boston, MA
Contact: rachelharmon25@neco.edu

PURPOSE

- Lateral interactions in the retina, mediated primarily by horizontal and amacrine cells, are crucial for edge and contrast enhancement, high contrast visual acuity, adaptation to different illumination conditions, and chromatic information processing.
- Several diseases (e.g. glaucoma, age-related macular degeneration, retinitis pigmentosa) affect retinal layers where lateral interactions occur, disrupting normal visual processing and resulting in profound visual problems.
- However, there is no published ERG protocol to study these functional mechanisms objectively and *in vivo* in humans.
- Using frequency tagging and a stimulus resembling a natural scene, we have developed a novel ERG protocol to study the effect a surrounding stimulus (SS) has on a dead leaves-patterned stimulus (DLS).

METHODS

- The ERG stimulus consisted of a ring of 8 DLSs, 4° diameter each, and a SS of isotropic noise (Figure 1). Image statistics indicate that the stimulus' spatial frequency distribution follows that of natural scenes (Figures 2 and 3)
- The DLS rings presented at 2 retinal eccentricities (6° and 10°), were contrast-reversed at 7.5 reversals/sec (50% average contrast, 75 cd/m^2 mean luminance).
- The SS consisted of isotropic contrast-reversing noise (1 reversal/sec) of 0%, 25%, 50%, and 75% (75 cd/m^2 mean luminance).
- Stimuli were presented on a 48" LG OLED monitor (120 Hz). ERGs were recorded monocularly with undilated pupils (viewing distance of 50 cm), using an Espion system (Diagnosys, US) with amplifier bandwidth between 0.5-100 Hz.
- Sixteen young adults (mean age 25 ± 2 years) with normal ocular health and BCVA 20/20 or better in each eye, participated in the study, wearing their habitual correction.
- A DTL and skin electrodes were used per standard protocol. One hundred 1-sec sweeps were time-averaged for each SS condition.
- The amplitude of the 15 Hz harmonic of the Fourier-transformed ERG (Figures 4 and 5) was used to plot SS contrast-response curves for each DLS eccentricity.

METHODS cont'd

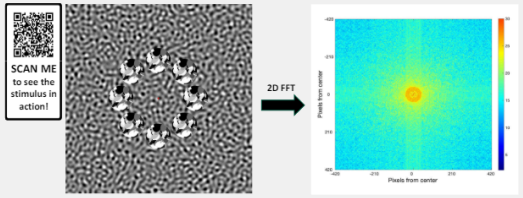

Figure 1: A ring of 8 DLSs at 6° eccentricity surrounded by the 75% contrast SS.

Figure 2: 2D FFT of Figure 1 showing the distribution of spatial frequencies throughout the image.

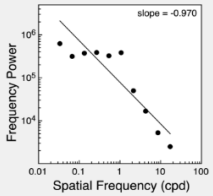

Figure 3: Spatial frequency content of Figure 1. Slope of approximately -1 indicates a natural image.

Figure 4: An ERG recorded with the DLS at 6° eccentricity and 75% SS contrast.

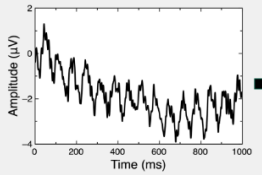

FFT

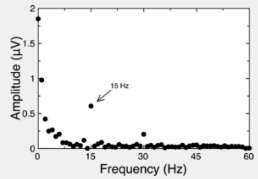

Figure 5: FFT of the ERG from Figure 4 showing increased response amplitude at 15 Hz.

RESULTS

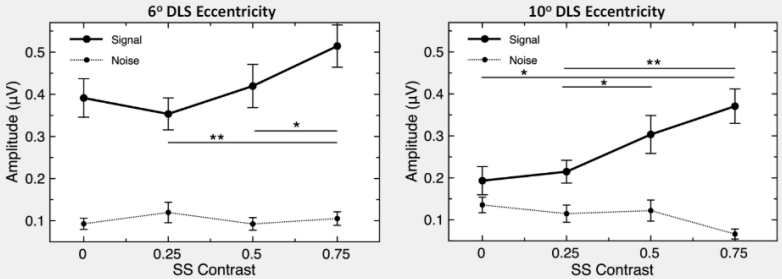

Figure 6 (left) and Figure 7 (right): Average FFT amplitude of the 15 Hz (Signal) and 14 Hz harmonics (Noise) as a function of SS contrast, for the 6° and 10° DLS eccentricities, respectively. Error bars depict ±1 SE. * p<0.05, ** p<0.001.

RESULTS cont'd

- Using repeated measures ANOVAs, we found a significant overall effect of SS contrast on the 15 Hz harmonic amplitude (6°: $p < 0.001$; 10°: $p < 0.001$).
- At 6° eccentricity, ERG amplitude increases significantly from 25% to 75% ($p < 0.001$) and from 50% to 75% ($p = 0.03$) SS contrast.
- At 10° eccentricity, ERG amplitude increases significantly from baseline to 75% ($p = 0.02$), from 25% to 50% ($p = 0.02$), and from 25% to 75% ($p < 0.01$) background contrast.
- ERG response amplitude is significantly higher at 6° eccentricity than at 10° eccentricity ($F=82.84$, $p < 0.001$).
- There is no effect of SS contrast on the phase of the ERG for either eccentricity.

CONCLUSIONS

- These results suggest that the contrast of the surrounding stimulus affects the retinal responses elicited by DLS stimulation, independent of luminance adaptation.
- This novel protocol will allow for analysis of lateral interactions in diseases, elucidating mechanisms that affect visual function, before apparent structural changes.
- Future studies should investigate psychophysical correlates of lateral interactions, along with VEPs elicited as a response to these stimuli.

REFERENCES

- Hubel DH, Wiesel TN. Receptive fields of optic nerve fibres in the spider monkey. J Physiol [Internet]. 1960 Dec 1;154(3):572–80.
- McCulloch DL, Kondo M, Hamilton R, Lachapelle P, Messias AMV, Robson AG, Ueno S. ISCEV extended protocol for the stimulus-response series for light-adapted full-field ERG. Doc Ophthalmol. 2019 Jun;138(3):205-215. doi: 10.1007/s10633-019-09685-8. Epub 2019 Mar 30. PMID: 30929108.
- Panorgias A, Aigbe S, Jeong E, Otero C, Bex PJ, Vera-Diaz FA. Retinal Responses to Simulated Optical Blur Using a Novel Dead Leaves ERG Stimulus. Invest Ophthalmol Vis Sci. 2021;62(10):1.
- Werblin FS, Dowling JE. Organization of the retina of the mudpuppy, Necturus maculosus. II. Intracellular recording. J Neurophysiol. 1969;32(3):339–55.

FUNDING & DISCLOSURES

- Funding: T35 Research Training Grant (5 T35 EY 7149-23), NECO Topcon Early Innovation Award, and NECO internal research funds.
- Disclosures: RH & TP Code N (No Commercial Relationships), FVD Code F (Reality Labs Research at Meta Platform Technologies, LLC).

Appendix 2: ARVO 2025 abstract and poster on psychophysical results

“Purpose: Lateral interactions play a critical role in retinal processing, but their role in myopia has not been fully assessed. We investigated the perception of stimuli in the presence of surrounding noise at 2 peripheral locations as a function of axial length.

Methods: Subjects (n = 35, avg 25 yrs, range 22-32 yrs) underwent a thorough vision screening, had BCVA 20/20 or better, and no ocular pathology or vision deficit other than refractive error (avg -2.97 D, range -6.88 to +1.15 D). Axial length (AXL) was measured using Lenstar (avg 24.97 mm, range 22.50-27.51 mm). Contrast Sensitivity (CSF) and Threshold versus Contrast (TvC) functions were measured at 6 deg and 10 deg eccentricities in an 8AFC task. Curves were acquired using adaptive thresholding (QuestPlus) with sine-wave gratings as targets. TvC curves were measured as a function of the contrast level of surrounding isotropic noise under both monocular and dichoptic conditions. Spearman-Rank correlations were analyzed as a function of AXL.

Results: From the CSF curves, negative correlations were found between AXL and acuity as well as the area under the low-frequency dropoff ($p = 0.045$) at 10 deg, but not at 6 deg eccentricity. Notably, no statistical significance was noted for the total area under the curve, location of the CSF peak, or the contrast sensitivity at the lowest spatial frequency (0..25c/deg). From the TvC functions, positive correlations were found under dichoptic conditions at 6 deg for the Area under the curve (AUTvC), contrast threshold at TvC minimum, and sensitivity to contrast changes (Psi). Under dichoptic conditions at 10 deg, the intrinsic noise of the visual system was positively correlated with AXL. No statistically significant correlations were noted under monocular conditions.

Conclusions: These findings suggest a possible relationship between axial length and center-surround interactions in the visual system. Notably, differences in monocular and dichoptic responses suggest a possible differential between cortical and retinal processing as a function of axial length.

This abstract was presented at the 2025 ARVO Annual Meeting, held in Salt Lake City, UT, May 4-8, 2025."

Reference:
Publication upcoming in IOVS June 2025

Figure 1. ARVO 2025 Poster

Psychophysical Analysis of Center Surround Interactions as a Function of Axial Length

2103 - A0283

NECO | New England College of Optometry

Rachel Harmon[1], Deepa Dhungel[1], Thanasis Panorgias[1], Peter J. Bex[2], Fuensanta A. Vera-Diaz[1]
[1]New England College of Optometry, Boston, MA [2]Northeastern University, Boston, MA

Contact: rachelharmon25@neco.edu

PURPOSE

- Lateral interactions are a key mechanism in visual processing, facilitating the creation of receptive fields, and are thought to be relevant in the emmetropization process.
- Previous work has demonstrated that mid-peripheral retinal eccentricities may be especially important in emmetropization, although the mechanism remains unknown.
- The present study addresses this gap by studying psychophysical correlates of lateral interactions at two mid-peripheral eccentricities in humans with a range of ocular axial length (AXL) values.

METHODS

- Subjects: N=35 young adults (age 25 ± 2 years), BCVA 20/20 or better in each eye, no ocular pathology or vision deficit other than refractive error (Avg -2.97D ± 2.36), wearing trial lenses with their best optical correction.
- Contrast Sensitivity (CSF) and Threshold versus Contrast (TvC) functions were measured at 6 and 10 deg eccentricity using adaptive thresholding (QuestPlus) with Gaussian sine-wave luminance gratings, 4 deg diameter, in an 8AFC task.
- CSF - the following outcomes were obtained: area under the log CSF (AULCSF), area under the low frequency dropoff (<0.50 cpd; AULCSF_LowPass), SF at the peak (SFpeak), CS at the peak (CSpeak), and high SF cutoff (Acuity).
- TvC - Surround stimulus consisted of isotropic noise of 0.04, 0.08, 0.16, 0.32, 0.64 contrast spanning a 2-10 deg ring. All gratings were presented with 4 cpd spatial frequency. Dipper functions were acquired with surround contrast level as the pedestal value under both monocular and dichoptic conditions (using circular polarization).
- TvC - the following outcomes were obtained: area under the TvC (AUTvC), intrinsic noise (IN), sensitivity to changes in contrast (Psi), contrast threshold at minimum (MinThresh), and pedestal contrast at minimum (MinPedes).
- Analysis: Spearman Rank correlations of specific outcomes with axial length (AXL).

METHODS/RESULTS: CSF

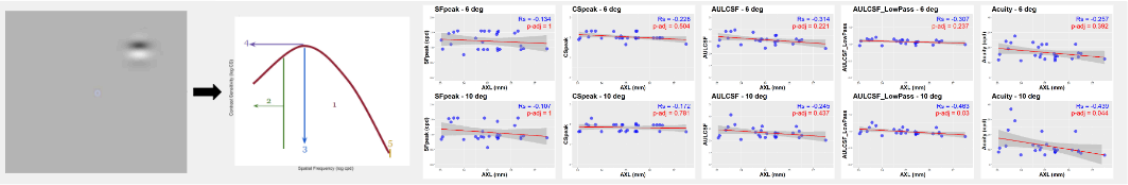

METHODS/RESULTS: TvC

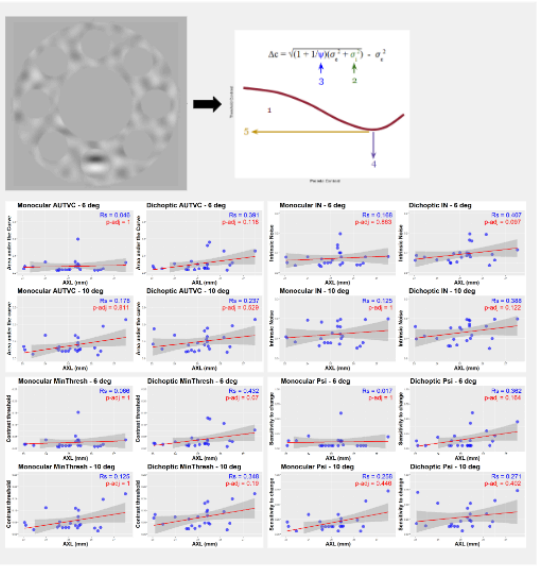

RESULTS cont'd

- No significant correlations were found between the peak spatial frequency (SFpeak), peak contrast sensitivity (CSpeak), or total area under the log CSF (AULCSF) and AXL at either eccentricity.
- A statistically significant negative correlation was found between the area under the low frequency drop off (lowpass filter set at 0.5 cpd; AULCSF_LowPass) and AXL at 10 deg (Rs = -0.463, p = 0.030), but not at 6 deg (Rs = -0.307, p = 0.237).
- Acuity showed a significant negative correlation with AXL at 10 deg (Rs = -0.439, p = 0.044), but not 6 deg (Rs = -0.257, p = 0.392).
- No significant correlations were found between TvC outcomes and AXL at either eccentricity or testing condition.

CONCLUSIONS

- Longer eyes tend towards lower contrast sensitivity at low spatial frequencies and lower spatial frequency cutoff values in the midperiphery.
- Promising correlations were noted at 10 degrees, but not 6 degrees eccentricity which supports future research probing visual function at 10 degrees.
- Further research is needed to investigate the role of lateral interactions in myopia development.

REFERENCES

- Panorgias A, Algbe S, Jeong E, Otero C, Bex PJ, Vera-Diaz FA. Retinal Responses to Simulated Optical Blur Using a Novel Dead Leaves ERG Stimulus.
- Smith EL, Ramamirtham R, Qiao-Grider Y, Hung LF, Huang J, Kee C su, et al. Effects of Foveal Ablation on Emmetropization and Form-Deprivation Myopia. Investig Opthalmology Vis Sci. 2007 Sep 1;48(9):3914.
- Taylor CP, Shepard TG, Rucker FJ, Eskew RT. Sensitivity to S-Cone Stimuli and the Development of Myopia. Investig Opthalmology Vis Sci. 2018 Sep 14;59(11):4622.
- Swiatczak B, Schaeffel F. Myopia: why the retina stops inhibiting eye growth. Sci Rep. 2022 Dec 15;12(1):21704.

FUNDING & DISCLOSURES

- Funding: T35 Research Training Grant (T35 EY7149-23), NECO Topcon Early Innovation Award, NECO Internal Research Funds.
- Disclosures: RH, DD, & TP Code N (No Commercial Relationships); FVD Code F (Reality Labs Research at Meta Platform Technologies, LLC); PJB Code C (Luminopia, Neurofieldz, Novartis) Code P (PerZeption, Adaptive Sensory Technology)